ISTANBUL TECHNICAL UNIVERSITY ★ GRADUATE SCHOOL

CALIX[4]PYRROLE-BASED SUPRAMOLECULAR ASSEMBLIES

M.Sc. THESIS

Mana MIRABOLGHASEMI

Department of Chemistry

Chemistry Programme

JUNE 2024

ISTANBUL TECHNICAL UNIVERSITY ★ GRADUATE SCHOOL

CALIX[4]PYRROLE-BASED SUPRAMOLECULAR ASSEMBLIES

M.Sc. THESIS

Mana MIRABOLGHASEMI
(509211264)

Department of Chemistry

Chemistry Programme

Thesis Advisor: Assoc. Prof. Dr. Abdullah AYDOĞAN

JUNE 2024

ISTANBUL TEKNİK ÜNİVERSİTESİ ★ LİSANSÜSTÜ EĞİTİM ENSTİTÜSÜ

KALİKS[4]PİROL TEMELLİ SUPRAMOLEKÜLER YAPILAR

YÜKSEK LİSANS TEZİ

Mana MIRABOLGHASEMI
(509211264)

Kimya Anabilim Dalı

Kimya Programı

Tez Danışmanı: Doç Dr. Abdullah AYDOĞAN

HAZİRAN 2024

Mana MIRABOLGHASEMI, an M.Sc. student of ITU Graduate School student ID 509211264, successfully defended the thesis/dissertation entitled "CALIX[4]PYRROLE-BASED SUPRAMOLECULAR ASSEMBLIES", which she prepared after fulfilling the requirements specified in the associated legislations, before the jury whose signatures are below.

Thesis Advisor :	**Assoc. Prof. Dr. Abdullah AYDOĞAN** Istanbul Technical University	.....
Jury Members :	**Assoc. Prof. Dr. Füsun Şeyma KIŞKAN** Istanbul Technical University	.....
	Prof. Dr. M. Kasım ŞENER Yıldız Technical University	.....

Date of Submission : 23 May 2024
Date of Defense : 25 June 2024

To my spouse,

FOREWORD

First and foremost, I express my heartfelt gratitude to my advisor, Assoc. Prof. Dr. Abdullah AYDOĞAN, for his support, encouragement, and guidance throughout my MSc journey.

I also would like to thank Prof. Dr. Aydan DAĞ and Assoc. Prof. Dr. Berkay SÜTAY for their valuable support on drug loading experiments and computational chemistry.

I extend my appreciation to my laboratory colleagues, Necla BEKTAŞ, Fatma Yelda ÜNLÜ, Deniz MEMIŞ, Hafize Reva BAYRAKTAR, and Ayşe ODABAŞ, for their support.

I am grateful to the Scientific Research Projects Unit of Istanbul Technical University (project code TYL-2022-44026) for their financial support, which has enabled me to pursue this research endeavor.

Lastly, I extend my deepest thanks to my parents, sister, and husband for their unwavering support and love. Their encouragement has been my source of strength throughout this endeavor.

June 2024

Mana MIRABOLGHASEMI
(Chemist)

TABLE OF CONTENTS

Page

ABBREVIATIONS

1-Br : Pyridinium Bromide Salt of Calix[4]pyrrole
1-Cl : Pyridinium Chloride Salt of Calix[4]pyrrole
1-F : Pyridinium Fluoride Salt of Calix[4]pyrrole
1-PF6 : Pyridinium Hexafluorophosphate Salt of Calix[4]pyrrole
AMP : Adenosine Monophosphate
Ant-Br : Bromo Anthracene
Ant-Py : Pyridinium Bromide Salt of Anthracene
BisPy : Bis pyridinium salt
C4P : Calix[4]pyrrole
C4P-Br : Bromo Calix[4]pyrrole
C4P-PEG : PEGylated Calix[4]pyrrole
C4P-PEG-DOX : Doxorubicin-Loaded PEGylated Calix[4]pyrrole micelles
CB7 : Cucurbit[7]uril
$CDCl_3$: Deuterated Chloroform
CLSM : Confocal Laser Scanning Microscopy
CMC : Critical Micelle Concentration
^{13}C NMR : Carbon Nuclear Magnetic Resonance Spectroscopy
DCC : Dicyclohexylcarbodiimde
DCM : Dichloromethane
DCU : Dicyclohexylurea
DLC : Drug Loading Capacity
DMAP : 4-Dimethylaminopyridine
DMSO : Dimethyl sulfoxide
DNA : Deoxyribonucleic Acid
DOX·HCl : Doxorubicin hydrochloride
EE : Encapsulation Efficiency
EtP5A : Perethylated Pillar[5]arene
FDA : Food and Drug Administration
FT-IR : Fourier Transform Infrared Spectroscopy
^{1}H NMR : Proton Nuclear Magnetic Resonance Spectroscopy

HPLC : High Performance Liquid Chromatography

HR-ESIMS : High-Resolution Electrospray Ionization Mass Spectrometry

MeOH : Methanol

MIM : Mechanically Interlocked Molecule

NOESY : Nuclear Overhauser Effect Spectroscopy

PEG : Polyethylene Glycol

PPR : Pillararene-Based Pseudorotaxane

Py : Pyridinium

SEM : Scanning Electron Microscopy

TBAsub : Tetrabutylammonium Suberate

TEA : Triethylamine

TEM : Transmission Electron Microscopy

THF : Tetrahydrofuran

UV-vis : Ultraviolet-Visible Spectroscopy

SYMBOLS

$\mathbf{D_h}$ **:** Hydrodynamic Diameter

$\mathbf{V_s}$ **:** Specific Viscosity

LIST OF TABLES

Page

LIST OF FIGURES

Page

CALIX[4]PYRROLE-BASED SUPRAMOLECULAR ASSEMBLIES

SUMMARY

Supramolecular assemblies are known as large-scale and organized structures formed as a result of the self-assembly of smaller molecules through non-covalent interactions such as hydrogen bonding, van der Waals interaction, metal-ion coordination, and cation-π interactions. Within this framework, poly-pseudorotaxanes and micelles are considered as noteworthy examples of supramolecular assemblies that have shown various applications in materials science and drug delivery. The study of such assemblies and attempts to manipulate them to design novel structures can contribute to advancements in these fields. To date, in the field of supramolecular chemistry, numerous macrocyclic structures such as crown ethers, cucurbiturils, calixarenes, and cyclodextrins have been used in the formation of supramolecular amphiphiles and mechanically interlocked molecules.

Among these well-known macrocyclic structures, calix[4]pyrrole is known for its remarkable features, including its capability to acquire cone conformation upon binding to an anion, which facilitates ion-pair recognition and anion sensing through hydrogen bonding with anions. Calix[4]pyrrole is a molecule known for its ability to bind various ions in different ways due to its unique conformational features suitable for host-guest interactions. As a result, various types of calix[4]pyrrole systems have been developed to sense or extract ions and can exhibit different binding modes, enabling their use in synthesizing molecular machines.

The main goal of this thesis is to demonstrate the applications of calix[4]pyrroles and how they can be used in various areas such as in drug loading and release, in addition to the formation of poly-pseudorotaxane structures, owing to its anion and ion-pair recognition capabilities, respectively. Therefore, in this thesis, we present the innovative synthesis of a non-ionic surfactant built upon the calix[4]pyrrole framework, where a polyethylene glycol (PEG) moiety is introduced at one of its meso positions (**C4P-PEG**). This surfactant demonstrates the ability to form stable micelles in water. Additionally, it exhibits the capacity to encapsulate a chemotherapeutic cancer drug, doxorubicin hydrochloride (DOX·HCl), by recognizing its counter chloride anion in an aqueous environment. Following the characterization of the synthesized compound using NMR spectroscopy and mass spectrometry, its micelle formation ability in water is confirmed through TEM imaging, DLS and NMR spectroscopy. Furthermore, to assess drug-loading and release capabilities, we employed the nanoprecipitation method and utilized techniques such as TEM and DLS for characterization. Lastly, UV-vis spectroscopy is conducted to determine the compound's drug loading capacity, and its release behavior is examined under different pH conditions, revealing a preference for release under acidic conditions.

In addition to the pioneering study of drug delivery applications using the anion recognition property of calix[4]pyrrole, we synthesized the bromide salt of pyridinium-functionalized calix[4]pyrrole (**1-Br**), which can self-assemble into a supramolecular polymer through ion-pair recognition, serving as the axle of a poly-

pseudorotaxane, and perethylated pillar[5]arene (**EtP5A**) was successfully threaded as the wheels. Moreover, in our anion-controllable molecular motions study, we examined the changes in the properties of the proposed poly-pseudorotaxane by substituting bromide ions in **1-Br** with fluoride (**1-F**), chloride (**1-Cl**), and hexafluorophosphate (**1-PF6**) ions using different characterization methods.

KALİKS[4]PİROL TEMELLİ SUPRAMOLEKÜLER YAPILAR

ÖZET

Supramoleküler kimya, makromoleküllerin oluşturduğu sistemler, bunların montajı ve kovalent olmayan etkileşimlere odaklanarak kimya biliminin temel bir parçası olarak ortaya çıkmıştır. Klasik kimya, öncelikle kovalent bağlar ve moleküllerle ilgilenirken, supramoleküler kimya, daha büyük ve daha karmaşık sistemlerin kovalent olmayan daha zayıf etkileşimler aracılığıyla nasıl oluştuğunu incelemektedir. Bu etkileşimler, hidrojen bağları, van der Waals kuvvetleri, metal-iyon koordinasyonu ve katyon-π etkileşimlerini içerir ve küçük moleküller büyük ölçekli, organize yapılar oluşturarak kendi kendine montajını sağlar. Bu montajlar, polipseudorotaksanlar ve miseller gibi, malzeme bilimi ve ilaç salınımında çeşitli uygulamalarda yer alır. Bu montajları incelemek ve yeni yapılar tasarlamak için manipüle etmek, bu alanlarda önemli ilerlemeler sağlayabilir. Supramoleküler moleküllerin özellikleri, kendilerini oluşturan bileşenleri veya bunların monte edildiği koşulları değiştirerek geliştirilebilir. Ayrıca, taç eterler, cucurbituriller, kaliksarenler ve siklodekstrinler gibi makrosiklik yapılar, supramoleküler amfifiller ve mekanik olarak kilitlenmiş moleküller oluşturmak için supramoleküler kimyada önemli rol oynarlar. Kovalent olmayan etkileşimler yoluyla stabil ev sahibi-konuk kompleksleri oluşturma yetenekleri, karmaşık ve işlevsel supramoleküler sistemlerin tasarım ve sentezini sağlar. Bu sistemler, ilaç salınımı, nanoteknoloji, malzeme bilimi ve moleküler makineler gibi çeşitli uygulamalara sahiptir.

Kaliks[4]pirol, işlevsel özellikleri ve çok yönlü uygulamalarıyla makrosiklik yapılar arasında öne çıkar. Seçici bağlanma özellikleri, florür, klorür, asetat ve fosfat gibi anyonların tanınması ve algılanmasında kullanılır. Bu yetenek, çevresel izleme ve biyomedikal uygulamalarda önemli yer turar.

Bu molekül, anyonlara bağlandığında konik bir konformasyon oluşur ve hidrojen bağları sayesinde iyon-çifti tanıma ve anyon algılama özelliği sağlanır. Dört pirol halkasının siklik düzenlemesiyle misafir molekülleri kapsamak için uygun bir boşluk oluşur. Elektron bakımından zengin pirol halkaları, anyonlara karşı güçlü bir afiniteye sahiptir ve bu da onun anyon tanıma ve algılama alanındaki kullanımını artırır. Ayrıca, kaliks[4]pirolün konformasyonel esnekliği, çevresel koşullara bağlı olarak çeşitli misafir moleküllere uyum sağlamasına izin verir. Bu uyum yeteneği, iyonların algılanması veya ekstraksiyonu için çeşitli kaliks[4]pirol sistemlerinin geliştirilmesini ve farklı bağlanma türleri ile moleküler makinelerin sentezinde kullanılmalarını sağlamıştır. Ayrıca, yeni çalışmalarda ilaç salınım uygulamaları için kaliks[4]pirol bazlı moleküller tasarlanmıştır. Bu makrosiklik moleküller, çeşitli dış uyarıcılara tepki verme yetenekleri ve çeşitli modifikasyonlara uyumları sayesinde supramoleküler polimerik sistemlerin ve jellerin sentezinde de yaygın olarak kullanılır. Bu özellikler, kaliks[4]pirolü supramoleküler kimyada son derece ilgi çekici bir konu haline getirir.

Supramoleküler olarak düzenlenmiş yapılar, hidrojen bağı, van der Waals etkileşimi, metal-iyon koordinasyonu ve katyon-π etkileşimi gibi kovalent olmayan etkileşimler aracılığıyla daha küçük moleküllerin kendi kendini düzenlemesi sonucu oluşan büyük ölçekli ve düzenli yapılar olarak bilinir. Bu çerçevede, poli-psedo-rotaksanlar ve miseller, malzeme biliminde ve ilaç taşınımı alanlarında çeşitli uygulamaları olan supramoleküler yapıların dikkate değer örnekleri olarak kabul edilir. Bu yapıların çalışılması ve bunları manipüle etme çabaları, bu alanlarda ilerlemelere katkı sağlayabilir. Şimdiye kadar, supramoleküler kimya alanında taç eterler, cucurbiturriller, kaliksarenler ve siklodeksrinler gibi birçok makrosiklik yapı, supramoleküler amfifilik ve mekanik olarak birbirine bağlı moleküllerin oluşumunda kullanılmıştır.

Bu bilinen makrosiklik yapılar arasında kaliks[4]pirol, bir anyon ile bağlandığında koni konformasyonunu elde etme yeteneği de dahil olmak üzere dikkate değer özellikleri ile bilinir. Bu sayede kaliks[4]piroller anyonlarla oluşturduğu hidrojen bağlarının yanı sıra iyon çifti reseptörü olarak da kullanılabilir. Kaliks[4]pirol, ev sahibi-misafir etkileşimlerine uygun benzersiz konformasyonel özellikleri nedeniyle farklı yollarla çeşitli iyonları bağlama yeteneği ile bilinen bir moleküldür. Sonuç olarak, çeşitli tipte kaliks[4]pirol sistemleri geliştirilmiş ve iyonları algılamak veya ekstrakte etmek için kullanılmıştır ve bu kaliks[4]pirol sistemleri farklı bağlanma modları sergileyebilir, ki bu da onların moleküler makinelerin sentezinde kullanılmalarının yolunu açabilir.

Kaliks[4]pirolün ilaç taşıma alanında yenilikçi yönü, anyonları tanıma ve bağlama yeteneğinde yatar, bu da ilaç taşıma sistemlerinin spesifikliğini ve verimliliğini artırmak için kullanılabilir. Kaliks[4]pirol yapısını değiştirerek, kapsüllenmiş ilaçların salınım sistemlerini özelleştirmek mümkündür, bu da onları kanser dahil çeşitli hastalıkların tedavisi için daha uygun hale getirir. Hidrofobik ilaçları kapsüle edebilen stabil miseller oluşturma yeteneği, ilaç taşıma alanındaki önemli zorluklardan biri olan terapötik ajanların biyolojik ortamlarda çözünürlüğü ve stabilitesi sorununa da çözüm sunar.

Bu tezin ana hedefi, kaliks[4]pirol türevlerinin uygulamalarını ve bunların ilaç yükleme ve ilaç salınımı gibi çeşitli alanlarda nasıl kullanılabileceğini, ayrıca anyon ve iyon-çifti tanıma yeteneklerine bağlı olarak psedo polirotaksan yapılarının oluşumunu göstermektir. Bu nedenle, bu tezde, polietilen glikol biriminin mezo pozisyonlarından birine dahil edilen kaliks[4]pirol çatısı üzerine kurulmuş iyonik olmayan yeni bir yüzey aktif maddenin sentezini sunmaktayız. Bu yüzey aktif madde, su içinde kararlı miseller oluşturma yeteneği göstermektedir. Ek olarak, su ortamında karşıt klorür anyonunu tanıyarak bir kemoterapötik kanser ilacı olan doksorubisin hidroklorürü (DOX·HCl) içine alma yeteneğine sahiptir. Sentezlenen bileşiğin karakterizasyonu, NMR spektroskopisi ve kütle spektrometrisi kullanılarak yapıldıktan sonra, su içindeki misel oluşum yeteneği, TEM görüntüleme, dinamik ışık saçılımı (DLS) ve NMR spektroskopisi ile doğrulanmıştır. Ayrıca, ilaç yükleme ve salınım yeteneklerini değerlendirmek için nano-çökeltme yöntemi kullanılmıştır ve karakterizasyon için TEM ve DLS gibi tekniklerden yararlanılmıştır. Son olarak, bileşiğin ilaç yükleme kapasitesini belirlemek için UV-Vis spektroskopisi ile ölçümü yapılmıştır ve salınım davranışı farklı pH koşullarında incelenmiştir, asidik koşullar altında salınımın tercih edildiği görülmüştür.

Kaliks[4]pirolün anyon tanıma özelliğinden yararlanarak ilaç taşıma uygulamalarının öncü çalışmalarına ek olarak, bu makrosiklik yapının piridinyum bromür tuzunu sentezledik, bu da iyon çifti tanıma yoluyla bir supramoleküler polimer oluşturabilir ve psedo polirotaksanın ekseni olarak kullanılabilir ve pillar[5]aren başarılı bir şekilde tekerlekler olarak eksene geçirilebilir. Ayrıca, anyon kontrollü moleküler hareketler çalışmamızda, farklı karakterizasyon yöntemleri kullanarak bromür iyonlarının florür, klorür ve hekzaflorofosfat iyonlarıyla değiştirilmesiyle önerilen poli-psedo-rotaksanın özelliklerindeki değişiklikler incelenmiştir.

Kaliks[4]pirol temelli sistemlere yönelik devam eden araştırmaların, gelecekte daha da yenilikçi uygulamalara yol açması beklenmektedir. Davranışlarını ve özelliklerini yöneten temel prensipler hakkındaki edinilen bilgiler arttıkça, bu sistemleri tasarlama ve kullanma stratejileri ortaya çıkacaktır. Bu, şüphesiz ki süpramoleküler kimyanın ilerlemesine ve çeşitli bilimsel ve teknolojik alanlara olan etkisine katkıda bulunacaktır. Kaliks[4]pirollerin ilaç taşıma, malzeme bilimi ve nanoteknoloji gibi alanlara büyük katkılar sağlama potansiyeli, bu heyecan verici kimya alanında devam eden araştırma ve geliştirmenin devamını sağlayacaktır.

1. INTRODUCTION

1.1 Supramolecular Assemblies

Inspired by the self-assembly processes observed in nature, scientists have explored the application of similar phenomena to synthesize complex structures employing a bottom-up approach. The final arrangement of these synthesized nanostructures such as micelles, vesicles, fibers, and nanotubes, etc. determines their unique properties, rendering them suitable for various applications such as drug delivery, bio-imaging, bio-sensing, and tissue engineering applications [1-3]. Additionally, supramolecular assemblies are known for their responsiveness to various external stimuli such as pH, temperature, and light or a combination of all of them owing to the presence of dynamic equilibrium. This property makes them intriguing targets for chemists and motivates their exploration of drug-delivery applications. Thus, with the assistance of supramolecular chemistry and the emergence of non-covalent interactions such as hydrogen bonding, π-π stacking, van der Waals forces, and electrostatic interactions, the design of novel structures with enhanced properties and unique applications is gaining momentum [4]. These non-covalent interactions play a crucial role in synthesizing supramolecular systems, including micelles and pseudorotaxanes, which represent two remarkable examples.

Moreover, macrocyclic structures such as cyclodextrins, pillararenes, cucurbiturils, and calixarenes have emerged as molecules with promising features for engaging in host-guest interactions, enabling the formation of supramolecular assemblies (Figure 1.1).

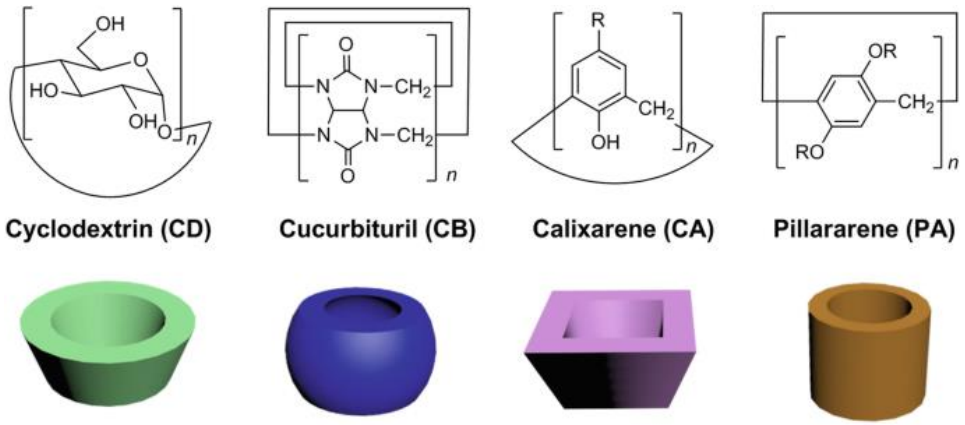

Figure 1.1 : Schematic representation of macrocyclic hosts.

A real example of using host-guest chemistry is mentioned when J.E Trend et al tried to solve the problem of finding the best method for assaying blood K^+. Eventually, the field of supramolecular chemistry blossomed by host-guest chemistry including the encapsulation of metal ions using crown ethers and small molecules to larger hosts [5, 6].

1.2 Micelles

Numerous anti-cancer drugs have been employed in cancer treatment, yet they possess inherent limitations prompting scientists to seek innovative approaches for enhancing their efficacy. In this pursuit, supramolecular chemistry has emerged as a pivotal discipline focusing on non-covalent interactions, leading to the development of novel structures aimed at refining cancer treatment with greater efficacy and selectivity. Common drawbacks such as poor solubility, adverse side effects, and limited bioavailability of cancer therapeutics necessitate acknowledgment [7]. One such advancement is the utilization of micelles, which address issues such as cytotoxicity through controlled-release mechanisms and enhanced responsiveness of supramolecular structures.

Micelles, recognized as monolayers consisting of amphiphilic structures formed through a spontaneous association known as self-assembly, have attracted considerable attention for their potential applications in drug delivery and food technologies (Figure 1.2). This attention stems from their diverse features and properties, which vary in accordance with their shapes, sizes, and biocompatibility.

In various environments and applications, the hydrophobic and hydrophilic components of micelles can arrange themselves into spherical structures through self-assembly. In an aqueous medium, the hydrophilic shell typically forms the outer layer, while the hydrophobic core has the ability to trap hydrophobic drugs. The flexibility in micelle design offers opportunities to address current challenges, including the poor solubility of small-sized micelles, low-loading capacity, and limited in vivo stability. Chemists are actively working to overcome these challenges, which could potentially enable the utilization of micelles in clinical applications [8].

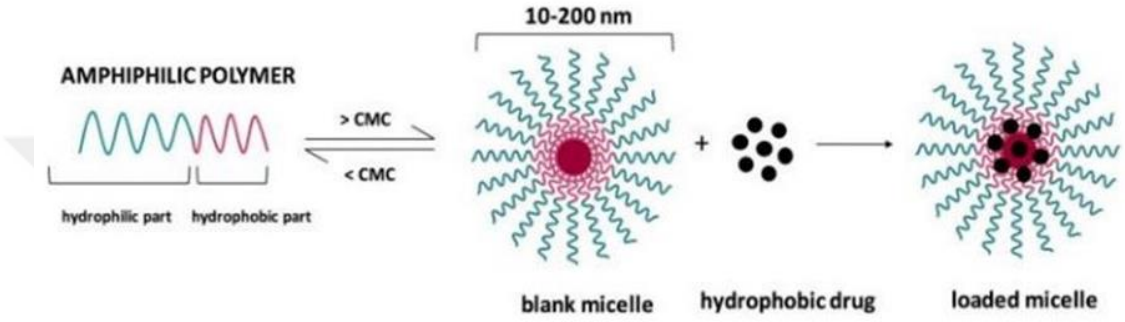

Figure 1.2 : Illustration of polymeric micelles formation.

Micelles exhibit various structures, with polymeric micelles being particularly significant. Their structure depends on the solvent in which they exist, and they can self-assemble into ordered configurations such as spherical micelles and vesicles once a specific concentration threshold, known as the critical micelle concentration (CMC), is attained. CMC holds great importance because when it's lower, it becomes much easier to prepare micelles, and the micelles formed are more stable as well. Low CMC ensures the stability of micelles, especially as they encounter further dilution within the body. This quality makes micelles with low CMC particularly favorable for drug-loading and release studies [9].

In designing micellar systems, it's imperative to note that improving circulation presents another significant challenge that demands attention in the pursuit of more effective cancer treatments. Therefore, in the design of micelles which are essentially tiny spherical clusters, using hydrophilic shells such as poly (ethylene glycol) (PEG) can effectively protect hydrophobic cores against the physiological conditions and extend their retention time in the blood by decreasing non-specific interactions with natural components and immune cells which is considered as one of the reasons for acquiring them in surfactant synthesis for drug delivery applications. PEG possesses

chemical properties such as hydrophilicity, anti-clotting ability, and solubility, and can resist protein adsorption; thus, it has been approved by the Food and Drug Administration (FDA) for clinical use [10].

1.3 Poly-Pseudorotaxanes

Pseudorotaxanes, functioning as an intermediate step in the synthesis of mechanically interlocked molecules (MIMs), involve the mechanical linkage of two components—an axle and a ring. These showcase unique characteristics, such as their responsiveness to external stimuli, making them vital candidates for a range of applications, especially in the design of molecular machines like rotaxanes. Although there have been numerous synthesized MIMs that are composed of macrocyclic molecules, there has been a focus on devising new strategies to synthesize pseudorotaxane structures based on non-covalent interactions composed of pillararenes. Recently, pillar[5]arenes have attracted attention in supramolecular chemistry field because of their remarkable features like straightforward functionalization, highly symmetric structure, and unique host-guest properties as a result of their electron-rich cavity which enable them to form stable complexes [11].

Additionally, calix[4]pyrroles are considered as a new generation of macrocycles that can be effectively used in ion-pair recognition due to their capability of binding to anions and cations at the same time by acquiring cone conformation which can extend supramolecular polymerization through a self-assembly process (Figure 1.3).

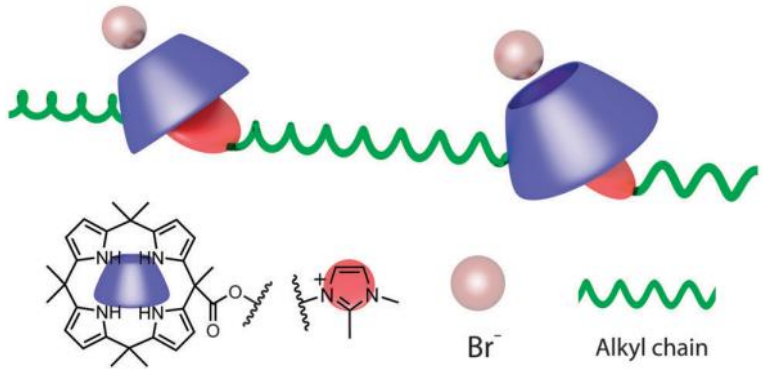

Figure 1.3 : Cartoon representation of supramolecular polymer formation through ion-pair recognition of bromide salt of imidazolium-functionalized calix[4]pyrrole.

One of the examples of using this phenomenon can be seen in Aydogan and Sessler's study where they synthesized a bromide salt of imidazolium functionalized

calix[4]pyrrole based on the ion-pair recognition of calix[4]pyrrole and the synthesized supramolecular polymer was examined using different characterization methods including ^{1}H NMR, DOSY and viscosity measurement [12].

Moreover, Valderrey and coworkers designed a [2]pseudorotaxane structure utilizing negatively polyatomic anions to create ion-paired complexes with a bis calix[4]pyrrole molecule. The proposed structure shows pseudorotaxane topology and can be controlled due to the ion-pair recognition property of calix[4]pyrrole [13]. This property was utilized in establishing the axle of a pseudorotaxane as Bektas and Aydogan did while synthesizing a poly-pseudorotaxane structure having a bis-pyridinium unit, BisPy, to activate the ion pair recognition property of calix[4]pyrrole, facilitating the establishment of an axle via linear supramolecular polymerization in the presence of TBAsub (Figure 1.4). Subsequently, pillar[5]arene was successfully threaded onto this structure. The threading of pillar[5]arene was promoted by dynamic non-covalent interactions between cations and π electrons within the calix[4]pyrrole cavity.

Figure 1.4 : Schematic representation of poly-pseudorotaxane formation via ion-pair recognition of calix[4]pyrrole using BisPy and TBAsub.

Polymerization commenced at a concentration of 31 mM, as determined by viscosity measurements. To characterize the proposed structure, various methods including ^{1}H NMR, (Nuclear Overhauser Effect Spectroscopy) NOESY, viscosity measurement, and DLS analysis were employed. Therefore, the ion-pair recognition concept was pragmatically used in the formation of mechanically interlocked molecules including poly-pseudorotaxanes [14].

1.4 Calix[4]pyrroles

Recent scientific fervor has surged around calix[4]pyrroles (**C4P**s), a class of macrocycles known for their facile functionalization and unique conformational changes. **C4P**s have been showing remarkable applications in diverse domains ranging

from separation and sensing to responsive materials and synthesizing supramolecular polymers due to their anion and ion-pair recognition properties which were extensively investigated by Sessler and colleagues [15]. **C4P**s were initially synthesized via an acid-catalyzed condensation reaction between pyrrole and a ketone. By varying the ketone employed, the functionalization of **C4P**s can be achieved [16]. Notably, among the four possible conformations for **C4P**- namely 1,2-alternate, 1,3-alternate, partial cone, and cone conformation - the latter has attracted significant attention from chemists. This is attributed to the unique cavity formed by the cone-shaped structure of **C4P**, which offers promising interactions with guest molecules. Specifically, in the presence of an anion, the cone conformation is favored (Figure 1.5). Subsequently, in the presence of a cationic species, interaction with **C4P** can occur via host-guest or cation-pi interactions, depending on the nature of the guest molecule [17].

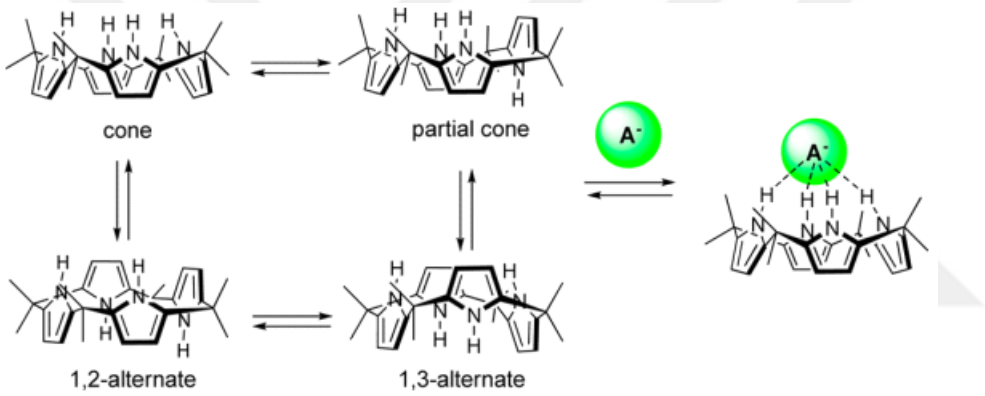

Figure 1.5 : Illustration of different conformations of calix[4]pyrrole being at equilibrium and favorable cone-shape formation in the presence of an anion.

This feature has led to many studies using **C4P** in the formation of supramolecular polymers, poly-pseudorotaxanes, micelles, and other supramolecular assemblies. Moreover, their easy-to-do modifiability can affect **C4P**s' binding performance which has motivated scientists to investigate synthesizing novel molecules based on them and diversify their applications in various fields, particularly in drug delivery. By functionalizing **C4P** and adding other moieties we can enhance its applications and properties and add more capabilities to the proposed structures in comparison to simple **C4P**s.

Considering that **C4P**s were investigated by Sessler and their capability for interacting with anions and neutral molecules was proved, using **C4P** in drug delivery applications was first mentioned by White et al. in 2013. Inspired by another study, where a SiO_2

stationary phase being used in HPLC was functionalized with calix[4]pyrrole and these molecules were able to separate peptides and oligonucleotides as negatively charged biomolecules, they envisioned that if **C4P** can interact with an anti-cancer drug it can be used as a transporter of that drug to DNA. For this purpose, the amino phenyl derivative of **C4P** was synthesized and was suitably utilized as a ligand in Pt(II) coordination (Figure 1.6). The delivery of Pt to DNA through **C4P** assistance was further examined using adenosine monophosphate (AMP) as a model compound instead of DNA and it was hypothesized that the delivery of Pt to DNA could occur based on the anion bonding of **C4P** and phosphate anion in the AMP structure. Although **C4P** did not show any interaction with phosphate in water, they showed cytotoxicity activity in the presence of cancer cells as a result of both trans-Pt(II) fragment and **C4P** being present [18,19].

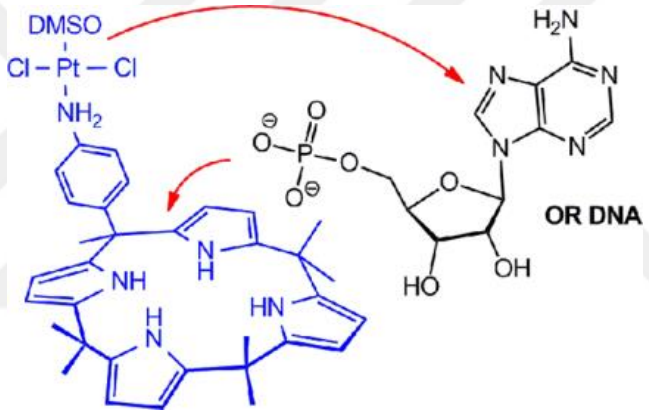

Figure 1.6 : Illustration of Pt complex delivery to the model molecule AMP through phosphate bonding of amino phenyl derivative of calix[4]pyrrole.

Subsequent studies, including the investigation of the acetamido phenyl version of **C4P** in 2018 showing high cytotoxicity towards cancer cells, have continued to advance our understanding of application in drug delivery. These studies highlight the potential of **C4P** to interact with anti-cancer drugs, facilitating targeted delivery and controlled-release mechanisms [20].

According to all these studies and knowing that chloride can induce a structural conformation known as cone conformation that enables the interaction between the positively charged segment of DOX·HCl and the **C4P** cavity through a type of interaction known as host-guest interaction, we have pioneered the development of a functional amphiphilic **C4P** system with desired loading capacity and favorable release under acidic condition.

1.5 Purpose of Thesis

In the literature, there are various examples of amphiphilic molecules comprising different macrocycles that have been actively utilized for drug release and encapsulation by means of the recognition of neutral or cationic guest moieties in aqueous media. However, to date, there has been no investigation into drug loading and release using calix[4]pyrrole based on anion recognition phenomena. This thesis aims to address this gap by presenting a nonionic calix[4]pyrrole compound designed as an amphiphilic system capable of forming micelles in water with high stability and exploring its potential as a drug-loading system. The proposed structure incorporates a PEG chain as the hydrophilic component attached to one of the meso positions of calix[4]pyrrole. Furthermore, Here in this thesis, we report a novel poly-pseudorotaxane using a calix[4]pyrrole-based supramolecular polymer in the axle that its driven force is the ion-pair recognition of calix[4]pyrrole and using perethylated pillar[5]arenes as the rings. In poly-pseudorotaxane formation, the concept of using calix[4]pyrrole's ion-pair recognition was previously used although the established system had some defects and limitations including very low solubility in higher concentration; therefore, our goal has been to address these shortcomings.

1.6 Literature Review

In this section of the thesis, some examples of supramolecular assemblies with their properties and applications were discussed:

The first study is about synthesizing a pillar[5]arene-based amphiphile using PEG as its hydrophilic moiety which was capable of forming micelles at low CMC, and nanoaggregates showed the noticeable capability of drug loading through guest encapsulation, and favored release in the presence of L-Asparagine, which was used to mimic the cathepsin B to investigate the hydrolysis of amide bonds (Figure 1.7). Accordingly, the dissociation of micellar carriers can occur in the presence of amide-cleaving enzymes, which can make them well-regarded to be efficiently used in anti-cancer drug release due to their selective enzyme responsiveness. In this study, various characterization methods such as NMR, DLS, TEM, and CLSM imaging were used to investigate the properties of the proposed structure and its behavior regarding doxorubicin encapsulation and release [21].

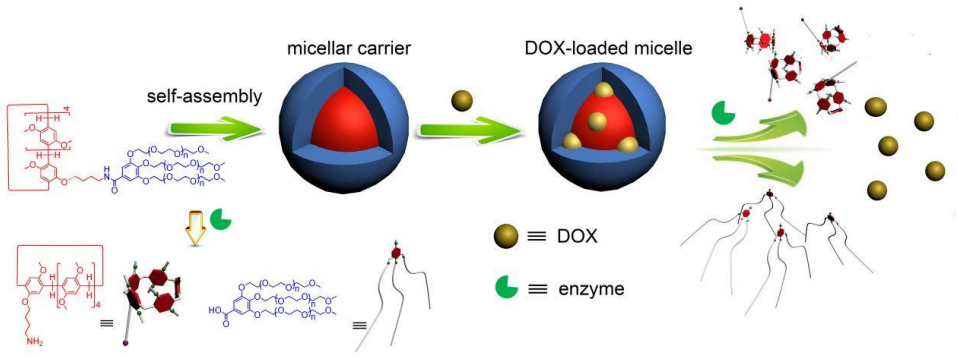

Figure 1.7 : Schematic representation of enzyme responsiveness of the DOX-loaded micelles.

The next study is about synthesizing an amphiphilic pillar[5]arene-based pseudo[1]rotaxane (PPR), which possesses a disulfide bond in the hydrophobic core, and PEG is used as the hydrophilic sector, showed the capability of self-assembling into spherical vesicles in aqueous solution (Figure 1.8). Their proposed structure showed favorable drug-loading capacity of 21.3 % and controlled release only in the presence of high concentration of Glutathione enzyme which could open new doors for accessing PPR in supramolecular amphiphilic structures showing responsiveness to specific enzymes. The role of pillar[5]arene is to encapsulate doxorubicin and protect the existing disulfide bond in the structure which prevents any unnecessary leakage of doxorubicin and enhances its targetability. Several characterization methods including NMR, TEM, DLS, CCK-assay, and fluorescence microscopy to analyze the synthesized structure and its drug loading and release capability in addition to its biocompatibility [22].

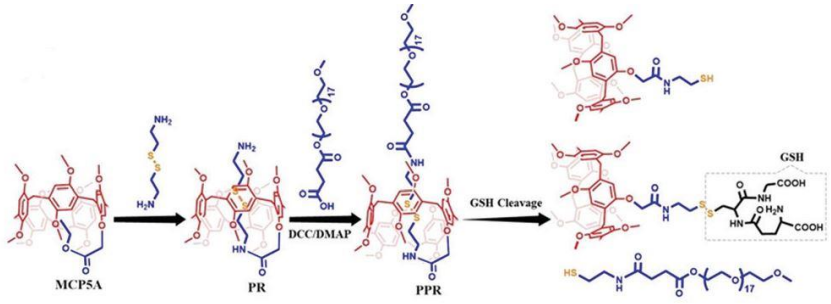

Figure 1.8 : Synthesis of the pseudorotaxane based on pillar[5]arene and its responsiveness towards glutathione, resulting in the release of DOX through the breakage of disulfide bond.

In this study, Sessler and colleagues introduced a thermoresponsive amphiphilic calix[4]pyrrole-based polymer designed to directly extract cesium anions from water due to its anion sensing property as a result of hydrogen bonding through its cone conformation, eliminating the need for organic solvents which showed potential to be used in water purification processes (Figure 1.9). Moreover, the polymer can be easily separated from water through heating, facilitating its recycling. Accordingly, poly(N-isopropylacrylamide)-b-poly(calix[4]pyrrole-co-methyl methacrylate) or PNIPAM-b-P(C4P-co-MMA) as P1, along with P2 as a control compound lacking calix[4]pyrrole, were prepared. Upon addition to an anion-containing aqueous medium, it was anticipated to adopt a micelle-like structure due to the presence of both hydrophilic PNIPAM and hydrophobic P(C4P-co-MMA) chains. The self-assembly and thermal-responsive behavior of these polymers in water were examined using DLS, TEM, ^{1}H NMR spectroscopy, and turbidity measurements [23].

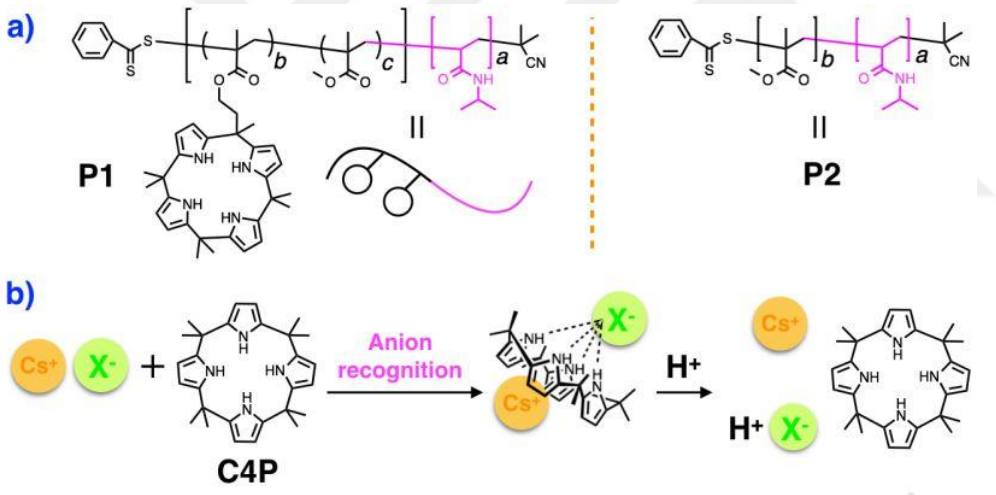

Figure 1.9 : (a) cartoon representation of P1 and P2 (b) schematic representation of removing cesium anions through anion recognition of calix[4]pyrrole and releasing them in a slightly acidic condition.

A water-soluble supramolecular polymer incorporating cucurbituril (CB7) was synthesized, demonstrating an exceptional ability to encapsulate the anti-cancer drug oxaliplatin with a loading efficiency of 12.1 w/w%. This was achieved by polymerizing bis-alkynyl functionalized CB7 with α,ω-diazide-PEG via a click reaction.

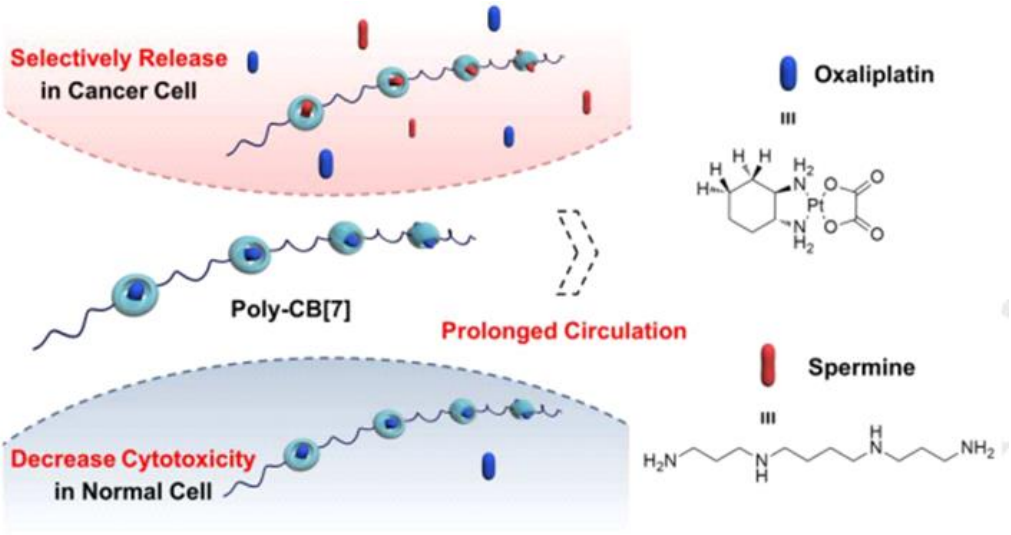

Figure 1.10 : Cartoon representation of CB7-based supramolecular polymer application in selective release of Oxaliplatin.

The polymer exhibited controlled-release of the anti-cancer drug triggered by the presence of spermine, a compound produced by cancerous cells. The level of spermine decreased due to competition with oxaliplatin which was encapsulated by CB7, resulting in oxaliplatin release and thereby enhancing the cytotoxicity against cancer cells. This mechanism underscores the potential of the polymer for targeted and efficient cancer therapy (Figure 1.10) [24].

Sessler et al. made significant progress by harnessing the ion-pair recognition property of **C4P** for various applications, particularly in the formation of amphiphilic supra structures (Figure 1.11). Through the implementation of dynamic covalent crosslinking methods, they induced self-assembly into multi-aggregated cross linkable micelles. These micelles demonstrated the remarkable capability to remove FeF_2 from water, marking a noteworthy advancement in the field. By incorporating aryl-extended **C4P**, which allows for easy functionalization on its aromatic sides, as a neutral macrocycle, they were able to create a polar head group based on ion-pair recognition, facilitating efficient self-assembly. Furthermore, the inclusion of 1,2,3-triazole linkers in the proposed structure (27) enabled effective metal cation complexation, thereby enabling the successful removal of FeF_2 from aqueous solutions [25].

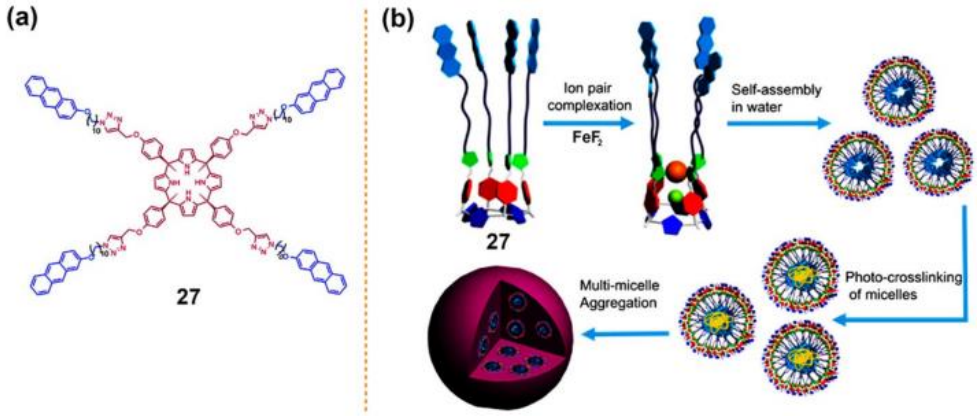

Figure 1.11 : (a) structure of 27 (b) Schematic representation self-assembly through ion-pair recognition of calix[4]pyrrole leading to higher-ordered aggregates.

In this study, pillar[6]arenes were utilized as threads, demonstrating superior attributes compared to pillar[5]arenes due to their larger cavities, and the backbone of polypseudorotaxanes can rely on non-covalent interactions, with the axle being a supramolecular polymer. This research employed metal coordination to establish the axle (Figure 1.12). Consequently, a [2]pseudorotaxane was initially synthesized, comprising a monoethylene oxide-substituted pillar[6]arene (P6) and guest (G) structure, resembling a paraquat derivative with two terminal cyano groups. These two molecules can interact, undergoing host-guest complexation, and subsequently coordinate with $AgSbF_6$ (Ag^+), leading to the formation of a polypseudorotaxane. The complexation between P6 and G was investigated using ^1H NMR and 2D NOESY to confirm the formation of the inclusion complex in the [2]pseudorotaxane. Next, a UV-Vis titration experiment was conducted to determine the association constant between P6 and G. Moreover, To confirm the formation of polypseudorotaxane, various methods were employed including ^1H NMR, DOSY, SEM, DLS, powder X-ray diffraction, and NMR titration [26].

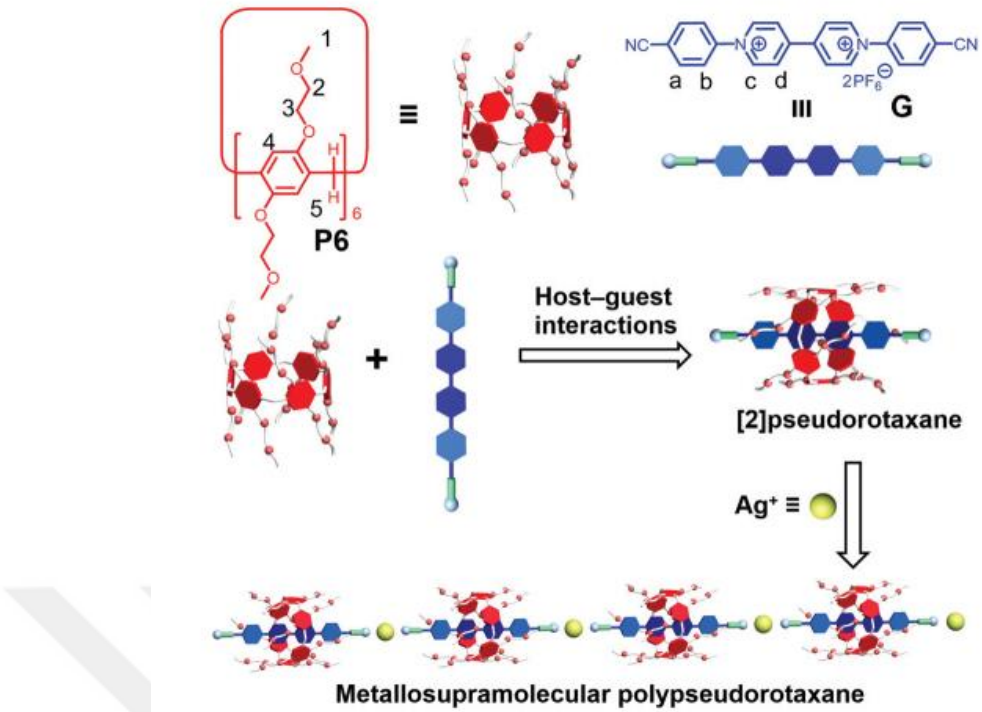

Figure 1.12 : Cartoon representation of metallosupramolecular formation by P6 and G monomers driven by metal coordination.

Hu and colleagues synthesized a side-chain polypseudorotaxane employing pillar[5]arenes, demonstrating its efficacy as an anion-responsive fluorescence sensor. Initially, they synthesized the conjugated polymer via a cu-catalyzed homocoupling reaction (Figure 1.13). Subsequently, they investigated the binding of this monomeric unit, which possessed two pillar[5]arene units, with n-octylpyrazinium hexafluorophosphate through host-guest interaction, employing ^{1}H NMR. The formation of the polypseudorotaxane was analyzed using fluorescence emission spectroscopy. The gradual addition of n-octylpyrazinium hexafluorophosphate led to a decrease in emission intensity due to electron transfer from the conjugated polymer. However, upon subsequent addition of chloride anion, the emission intensity increased, indicating the formation of an ion pair of n-octylpyrazinium chloride and the disassembly of the polypseudorotaxane structure. This responsiveness to anions highlights the potential utility of this synthesized structure [27, 28].

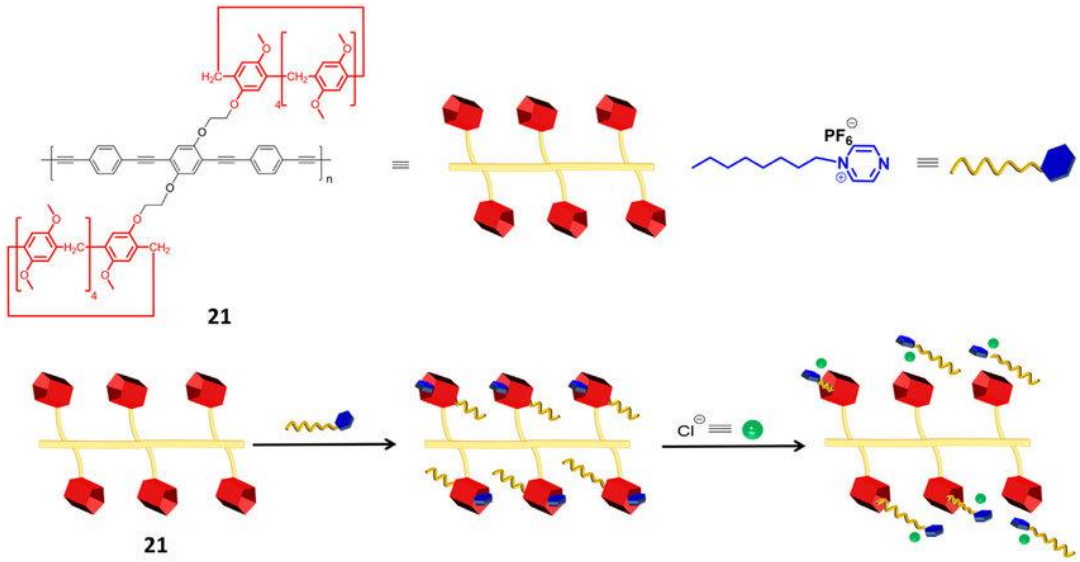

Figure 1.13 : Schematic representation of poly-pseudorotaxane formation and their disassembly by the presence of chloride anion.

Su and colleagues presented another instance of a poly[2]pseudorotaxane, which they synthesized by leveraging metal coordination interactions in DMSO. While most polypseudorotaxane structures typically form in low-polarity solvents or aqueous environments, the high polarity of solvents like DMSO poses a challenge due to its limitation on non-covalent interactions that was overcome in their study. Initially, a [2]pseudorotaxane comprising pillar[5]arene and bis(pyridinium)dicationic (1) was synthesized. Subsequently, polymerization via metal coordination was conducted utilizing $[PdCl_2(PhCN)_2]$ (Figure 1.14). The formation of this polypseudorotaxane was contingent upon various factors, such as monomer concentrations and temperature.

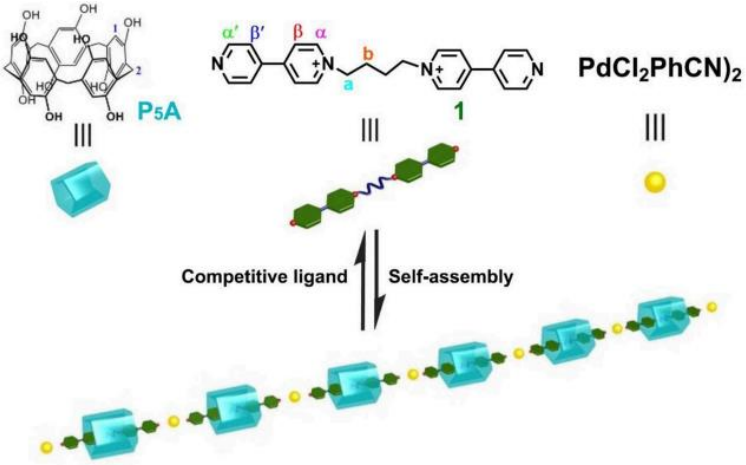

Figure 1.14 : Schematic representation pillararene-based poly-pseudorotaxane formation through metal-ion coordination.

Also, polymerization was observed to commence at a concentration of 51 mM in DMSO. At concentrations exceeding 500 mM, it exhibited the ability to form a supramolecular gel, which demonstrated responsiveness to temperature through a sol-gel transition. Various characterization techniques, such as ^{1}H NMR, NOESY, DOSY, SEM, and viscometry, were employed to investigate the complexations and polymerization characteristics [29].

2. EXPERIMENTAL

2.1 Materials

Methoxy polyethylene glycol (Aldrich), Succinc anhydrid (99%, Aldrich), 4-dimethylaminopyridine (99%, Aldrich), Toluene (99.7%, Aldrich), Triethylamine (Merck), Dichloromethane (DCM), Hydrochloric acid (37%, Merck), Sodium chloride (Aldrich), Sodium Sulfate (Merck), Petroleum Ether (J.T.Baker), Dimethyl amino pyridine (99%, Aldrich), N,N'-dicyclohexylcarbodiimide (Aldrich), Methanol (99%, Aldrich), Dimethylsulfoxide (Merck), Doxorubicin Hydrochloride (Aldrich), Tetrahydrofuran (THF, 99%, Aldrich), $CDCl_3$(99%, Aldrich), D_2O (Aldrich), Dimethylsulfoxide-d_6 (Merck), 10-bromodecanoic acid (Aldrich), Sodium Bicarbonate (Aldrich), 9-Anthracenemethanol (97%, Aldrich), 11-bromodecanoicacid (99%, Aldrich), Acetonitile (99.9%, Merck), Pyridine (Aldrich), Diethylether (IsoLab, 99.5%), Tetrabutylammoniumfluoride trihydrate (TBAF.$3H_2O$, 99%, Aldrich), Tetrabutylammonium chloride (97%, Aldrich), Amberlyst A26 hydroxide (Aldrich), potassium hexafluorophosphate (Aldrich) were purchased from commercial sources. All solvents were dried before use according to standard procedures. Unless specifically indicated, all other chemicals and reagents used in this study were purchased from commercial sources and used as received.

2.2 Instrumentation

^{1}H-, ^{13}C-, NOESY-, DOSY- NMR spectra were recorded on Agilent VNMRS 500 spectrometers using TMS as an internal reference at 25 °C. Mass spectra were measured on a Bruker Microflex LT MALDI-TOF mass spectrometer. UV-Vis spectra were carried out on a Shimadzu UVmini-1240 Spectrophotometer. Transmission electron microscopy (TEM) images were obtained by Hitachi HT7800 with EXALENS (120 kV). Nanoparticle sizes (the average hydrodynamic diameters and size distributions of the prepared nanoparticle solutions) were determined using a Malvern Zetasizer Nano ZS particle size analyzer equipped with a 4 mV He-Ne laser operating at λ = 632 nm, an avalanche photodiode detector with high quantum

efficiency, and an ALV/LSE-5003 multiple tau digital correlator electronics system. Samples were prepared at a concentration of 1 mg/mL in ultrapure water and purified from dust using a microfilter (0.45 μm) before the measurements. Viscosity measurements were carried out with an Ubbelohde micro dilution viscometer (Shanghai Liangjing Glass Instrument Factory, 0.40 mm inner diameter) at 293 K. Melting points were determined using a Stuart SMP10 instrument with 1 °C/min temperature increment under ambient conditions.

2.3 Synthesis and Characterization

Alcohol-functionalized calix[4]pyrrole and perethylated pillar[5]arene were synthesized according to the previous papers [30, 31].

2.3.1 Synthesis of *m*PEG-COOH

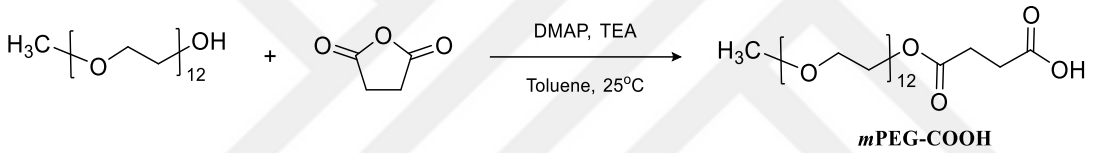

***m*PEG-COOH**

*m*PEG-OH (methoxy polyethylene glycol, Mn = 550 g/mol, 500 mg, 0.89 mmol), succinic anhydride (134 mg, 1.34 mmol), and 4- dimethyl aminopyridine (10.9 mg, 89 μmol) were dissolved in anhydrous toluene (2.5 mL). After stirring for 15 minutes, the mixture was added to triethylamine (124 μL) dropwise. The crude solution was stirred for 40 hours in a vial at 25 °C under an N_2 atmosphere. Toluene was evaporated from the reaction mixture and 20 ml DCM + 30 ml water + 2 ml HCl (2M) were added. The obtained organic mixture was washed with 2 x 50 ml saturated NaCl solution. The organic mixture was dried with Na_2SO_4. Following this, precipitation in petroleum ether afforded the product as a viscous liquid (290 mg, 49 %). ^{1}H NMR (500 MHz, $CDCl_3$) δ = 4.30 – 4.24 (m, 2H), 3.67 (d, J = 15.4 Hz, 44H), 3.56 (dd, J = 5.9, 3.5 Hz, 2H), 3.39 (s, 3H), 2.69 – 2.60 (m, 4H). ^{13}C NMR (126 MHz, $CDCl_3$) δ = 174.2, 172.1, 77.3, 77.0, 76.8, 71.9, 70.7, 70.6, 70.5, 69.0, 63.8, 59.0, 29.7, 29.5, 29.0.

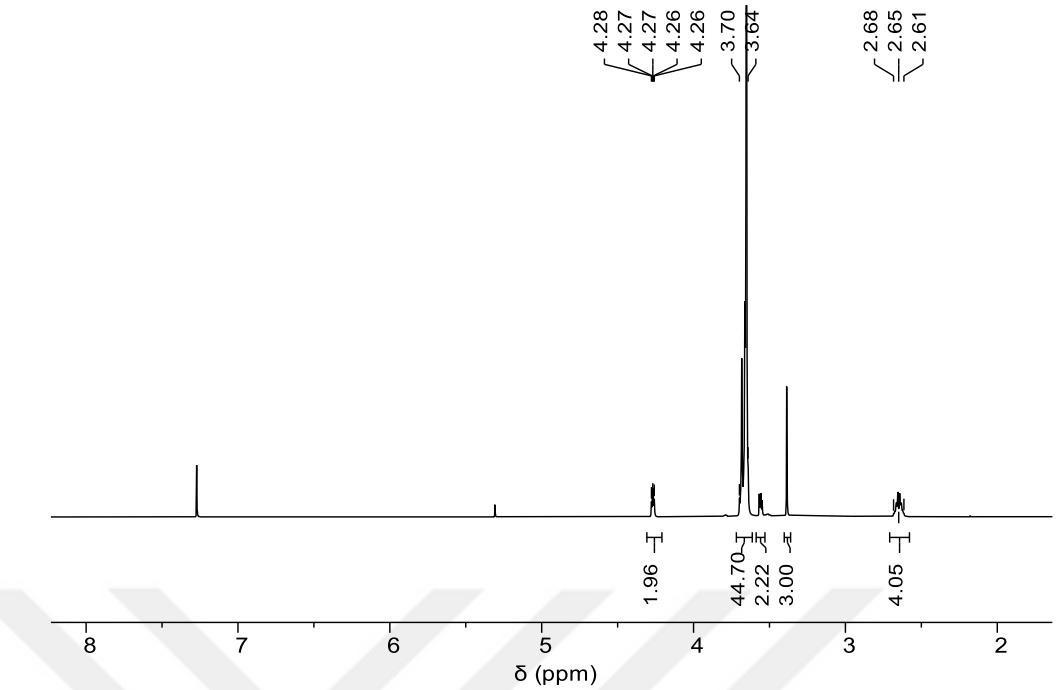

Figure 2.1 : ^{1}H NMR spectrum of *m*PEG-COOH recorded in $CDCl_3$ at 25 °C.

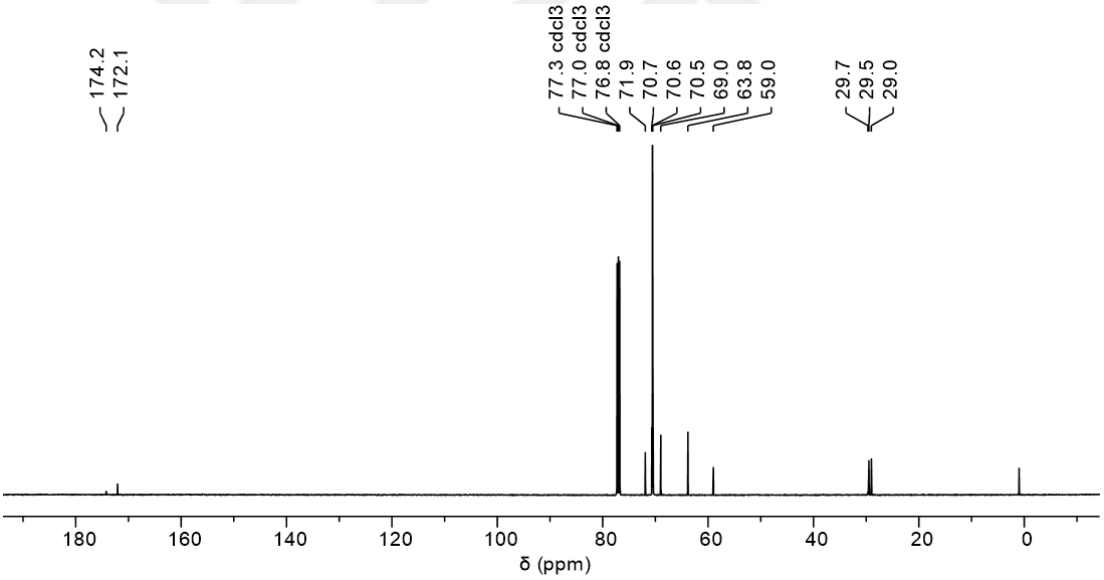

Figure 2.2 : ^{13}C NMR spectrum of *m*PEG-COOH recorded in $CDCl_3$ at 25 °C.

2.3.2 Synthesis of C4P-PEG

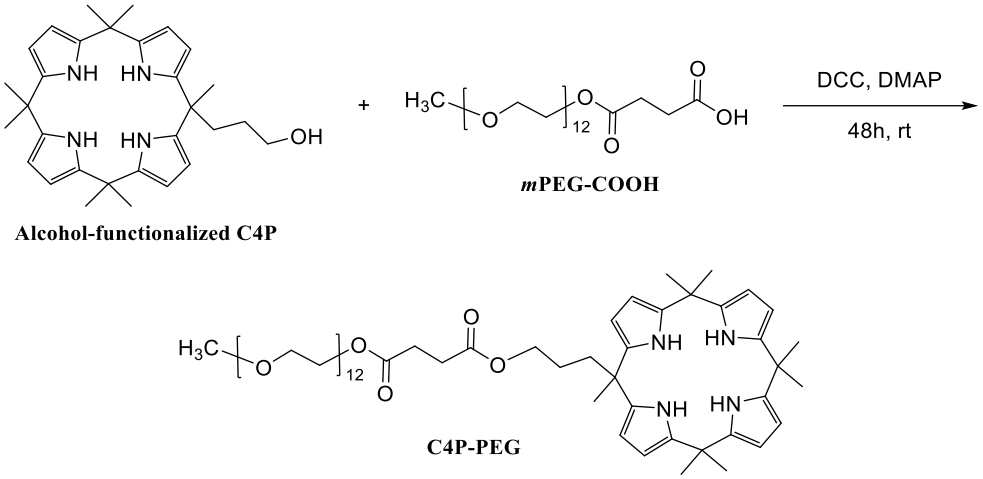

To a solution of *m*PEG-COOH (581 mg, 879.30 µmol), 4-dimethylaminopyridine (107.43 mg, 879.30 µmol) and alcohol-functionalized calix[4]pyrrole (540.31 mg, 1.14 mmol) in 8 ml of anhydrous dichloromethane (DCM), dicyclohexylcarbodiimide (DCC) (272.14 mg, 1.32 mmol) was added dropwise. The mixture was stirred at room temperature for 48 hours while being protected from light. After this period, the insoluble byproduct, dicyclohexylurea (DCU), was removed through suction filtration. Next, the mixture was placed in a deep freeze for an additional 4 hours to facilitate the removal of any remaining DCU, which was extracted in the same manner. The next step involved purifying the mixture via column chromatography (2 % MeOH/DCM). The final product obtained from this process is a yellow, viscous liquid (163 mg) with a yield of 16.6 %. ^{1}H NMR (500 MHz, $CDCl_3$) δ = 7.09 (s, 4H), 5.92 – 5.86 (m, 8H), 4.25 – 4.19 (m, 2H), 3.98 (t, J = 6.5 Hz, 2H), 3.72 – 3.62 (m, 40H), 3.58 – 3.53 (m, 2H), 3.39 (s, 3H), 2.65 (dd, J = 6.0, 1.1 Hz, 4H), 2.60 (ddd, J = 8.0, 6.0, 1.5 Hz, 2H) 1.91 – 1.85 (m, 2H), 1.53 – 1.47 (m, 20H), 1.45 (s, 3H). ^{13}C NMR (126 MHz, $CDCl_3$) δ = 171.3, 171.2, 137.7, 137.5, 137.4, 135.9, 102.8, 101.8, 101.8, 101.7, 76.3, 76.0, 75.8, 70.9, 69.6, 69.6, 69.5, 68.0, 63.9, 62.8, 58.0, 37.5, 35.7, 34.2, 34.2, 31.5, 29.7, 28.2, 28.0, 28.0, 28.0, 25.1, 22.8.

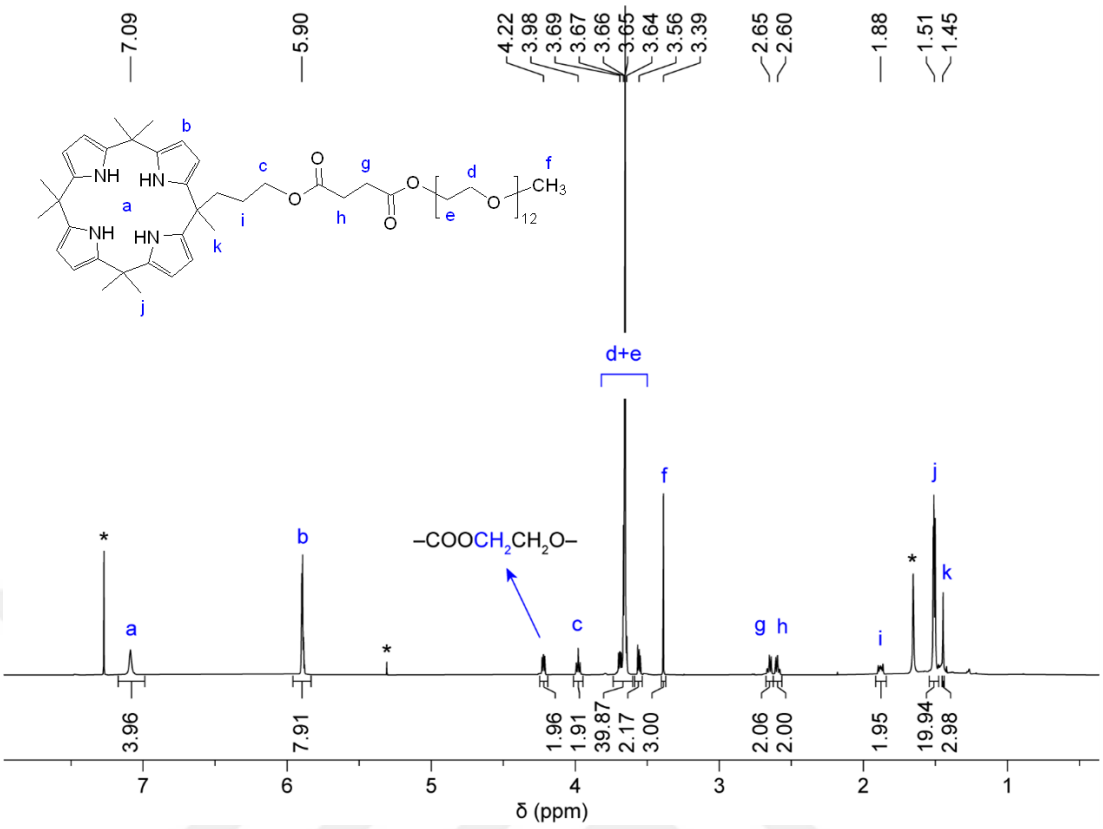

Figure 2.3 : ^{1}H NMR spectrum of C4P-PEG in $CDCl_3$ at 25 °C.

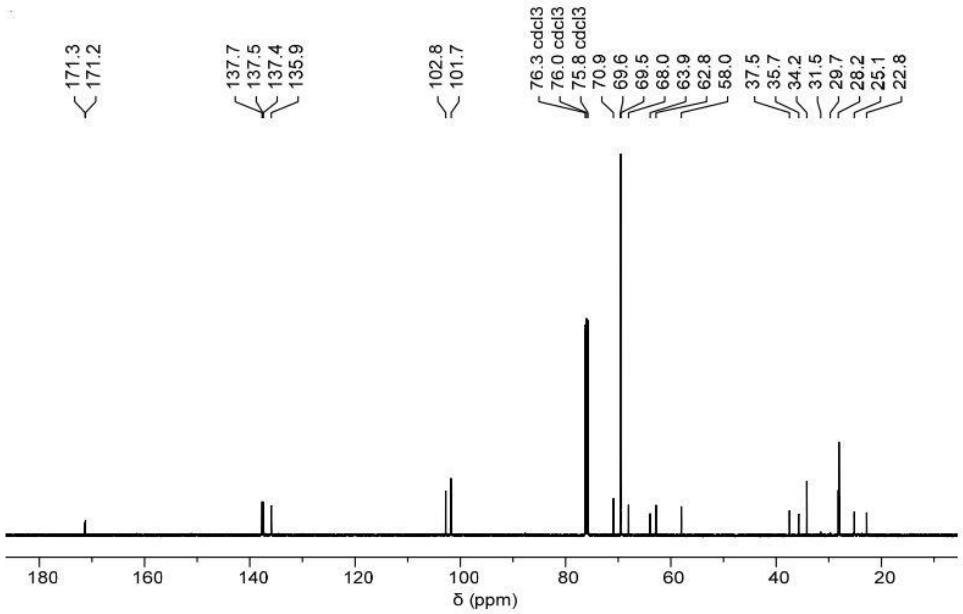

Figure 2.4 : ^{13}C NMR spectrum of C4P-PEG in $CDCl_3$ at 25 °C.

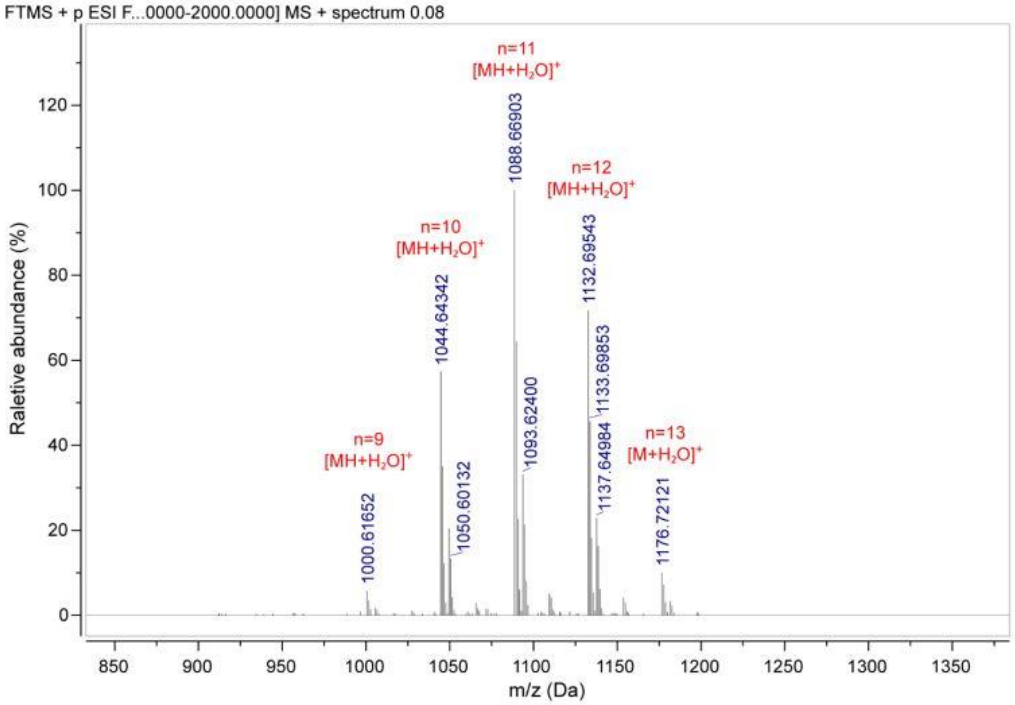

Figure 2.5 : HR-ESIMS spectrum of C4P-PEG.

2.3.3 Synthesis of Bromo Calix[4]pyrrole (C4P-Br) and Bromo Anthracene (Ant-Br).

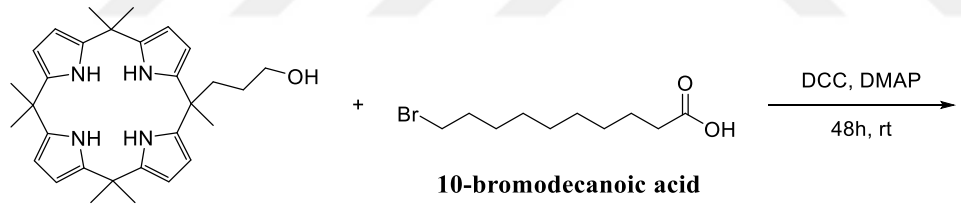

10-bromodecanoic acid

Alcohol-functionalized C4P

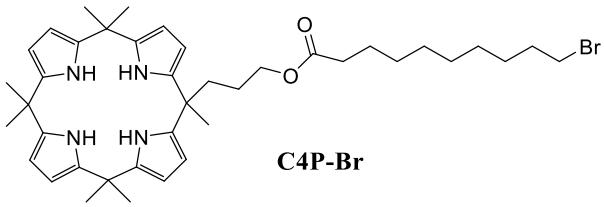

C4P-Br

To a solution of alcohol-functionalized calix[4]pyrrole (1.50 g, 3.17 mmol), 10-bromo decanoic acid (876.75 mg, 3.49 mmol) and 4-dimethylaminopyridine (38.77 mg, 317.34 µmol) in dichloromethane (25 mL), N, N'-Disyclohexylcarbodiimde (720.26 mg, 3.49 mmol) was added dropwise. The reaction stirred for 2 days at 25 °C while being protected from light. Next, the mixture was washed with cold DCM and filtered off multiple times to remove the Dicyclohexylurea (DCU). Afterward, extraction was conducted using hydrochloric acid (0.2 N), saturated sodium bicarbonate, and distilled

water two times, respectively. The obtained solution was evaporated, dried, and further purified via column chromatography over silica gel (DCM) to obtain a yellowish-white solid (1.35 g, Yield: 60.14 %). M.p. 116-117 °C. ^{1}H NMR (500 MHz, $CDCl_3$) δ = 7.05 (d, J = 11.7 Hz, 4H), 5.93 – 5.87 (m, 8H), 3.95 (t, J = 6.5 Hz, 2H), 3.42 (t, J = 6.9 Hz, 2H), 2.27 (t, J = 7.5 Hz, 2H), 1.92 – 1.82 (m, 4H), 1.61 (q, J = 7.4 Hz, 2H), 1.53 – 1.49 (m, 18H), 1.48 – 1.41 (s, 3H), 1.31 (s, 10H). ^{13}C NMR (126 MHz, $CDCl_3$) δ = 174.0, 138.8, 138.6, 138.5, 137.0, 104.0, 103.0, 103.0, 64.6, 38.6, 37.0, 35.3, 34.5, 34.1, 33.0, 29.4, 29.3, 29.2, 28.8, 28.3, 26.3, 25.1, 24.0.

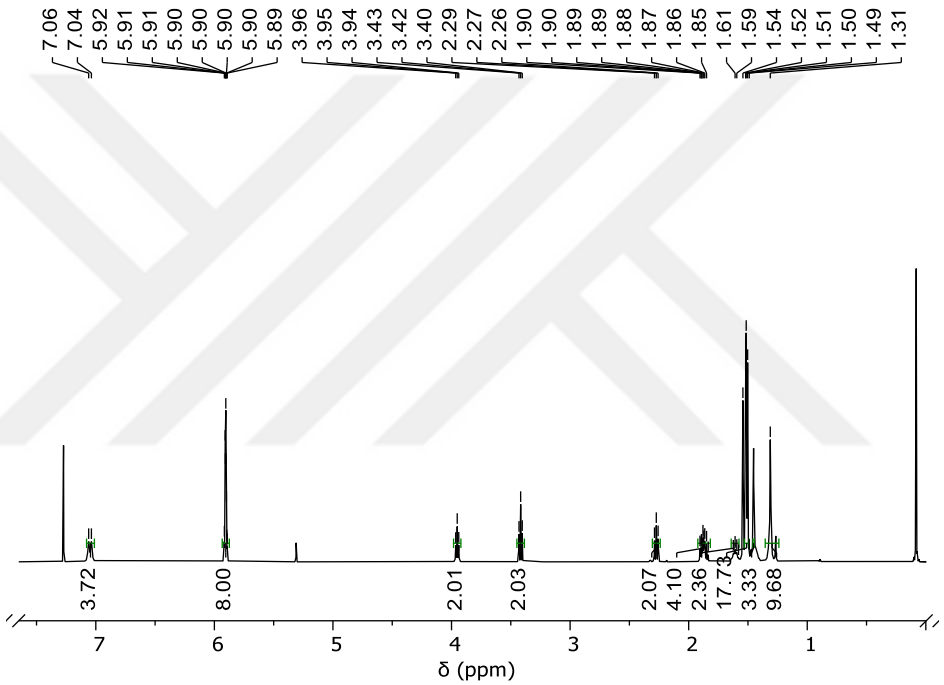

Figure 2.6 : ^{1}H NMR spectrum of C4P-Br in $CDCl_3$ at 25 °C.

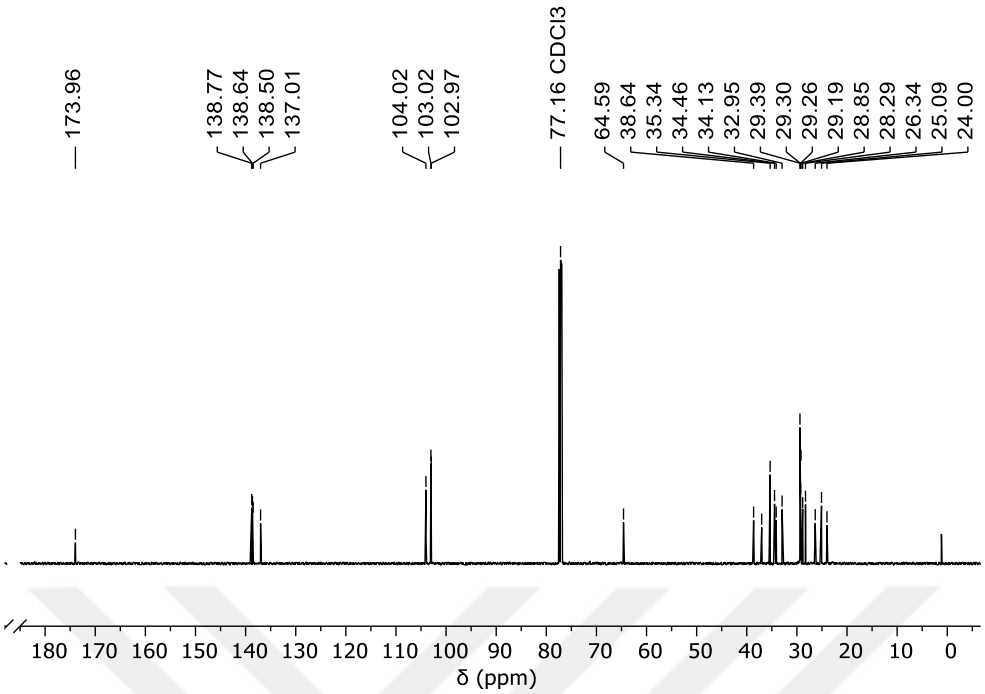

Figure 2.7 : ^{13}C NMR spectrum of C4P-Br in $CDCl_3$ at 25 °C.

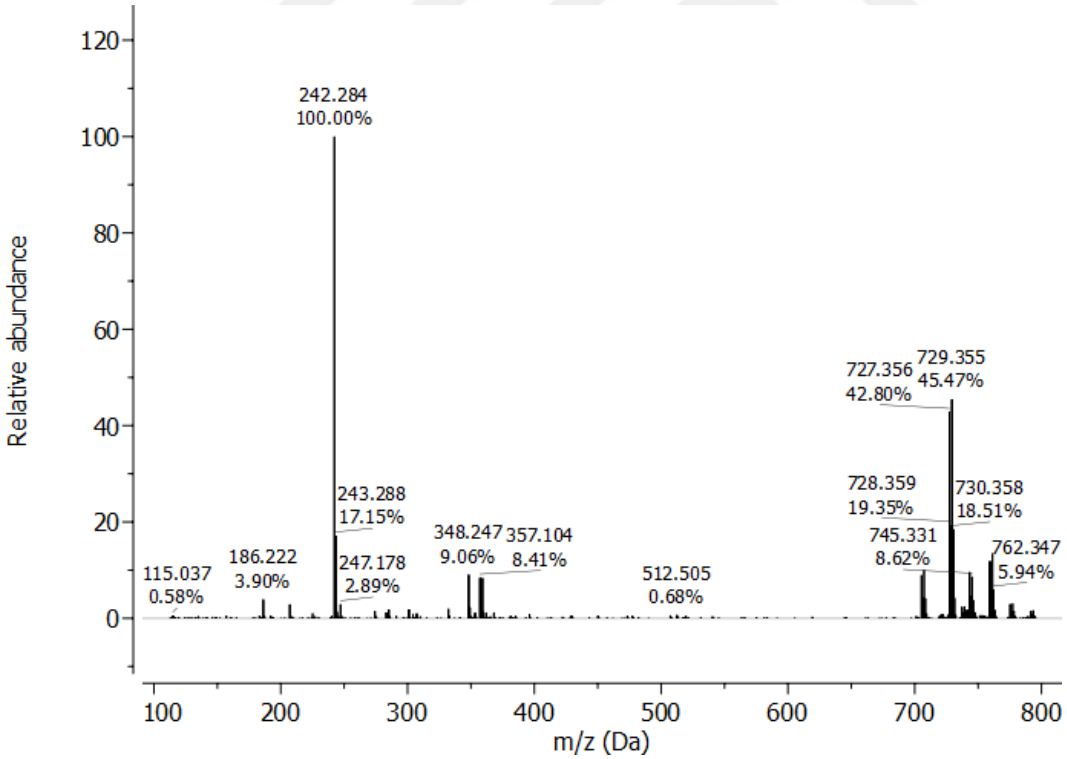

Figure 2.8 : Pos-HR-ESIMS of C4P-Br.

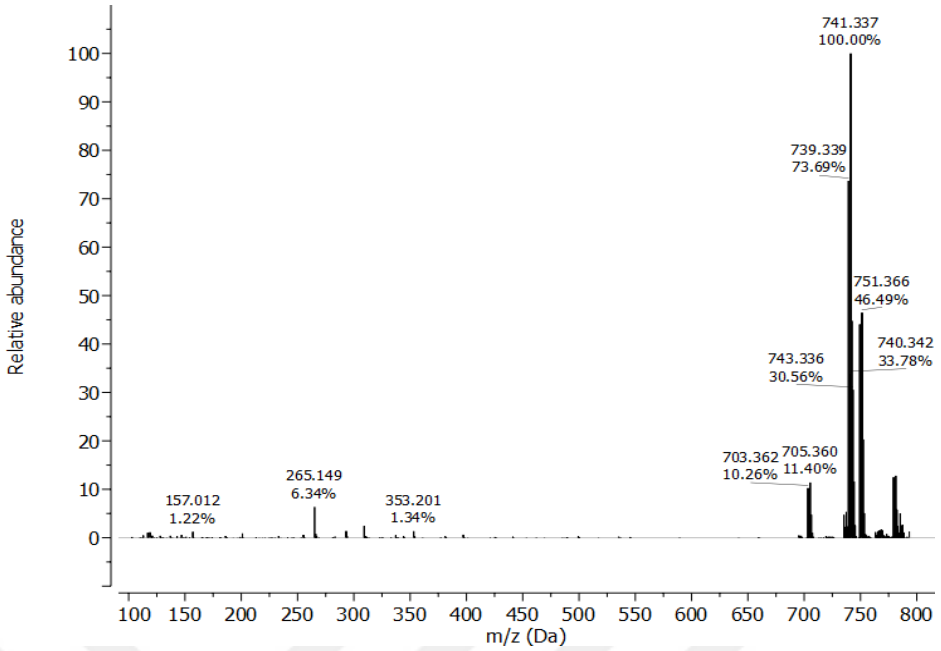

Figure 2.9 : Neg-HR-ESIMS of C4P-Br.

A similar procedure was used for bromo anthracene synthesis (651 mg, Yield: 74.42 %). 9-anthracenemethanol (400 mg, 1.92 mmol), and 11-bromoundecanoic acid (560.28 mg, 2.11 mmol) were mixed in DCM (8 mL) in the presence of DCC (435.93 mg, 2.11 mmol) and DMAP (23.47 mg, 192.07 µmol) as starting materials. M.p. 90-95 °C. ^{1}H NMR (500 MHz, $CDCl_3$) δ = 8.53 (s, 1H), 8.35 (d, J = 9.7 Hz, 2H), 8.05 (d, J = 8.4 Hz, 2H), 7.55 – 7.47 (m, 4H), 6.17 (s, 2H), 3.40 (t, J = 6.9 Hz, 2H), 2.34 (t, J = 7.5 Hz, 2H), 1.88 – 1.79 (m, 2H), 1.62 (p, J = 7.4 Hz, 2H), 1.39 (p, J = 7.2 Hz, 2H), 1.30 – 1.19 (m, 10H). ^{13}C NMR (126 MHz, $CDCl_3$) δ = 174.3, 131.6, 131.2, 129.3, 126.7, 126.6, 125.3, 124.1, 58.8, 34.5, 34.2, 33.0, 29.4, 29.4, 29.3, 29.2, 28.8, 28.3, 25.1.

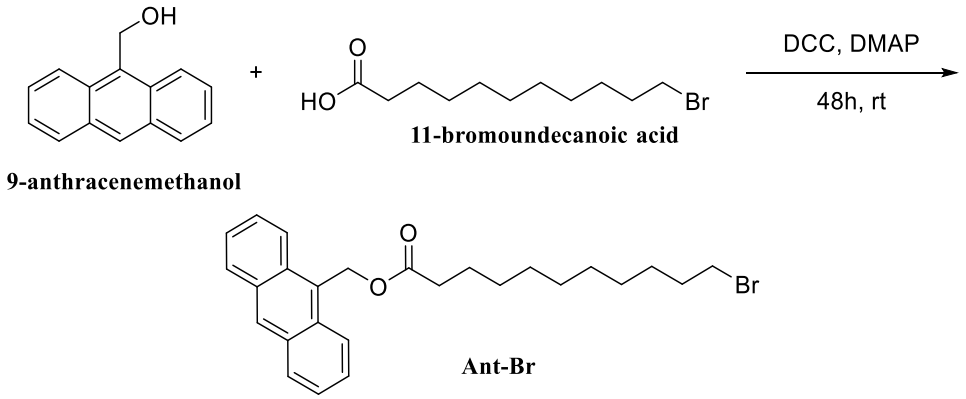

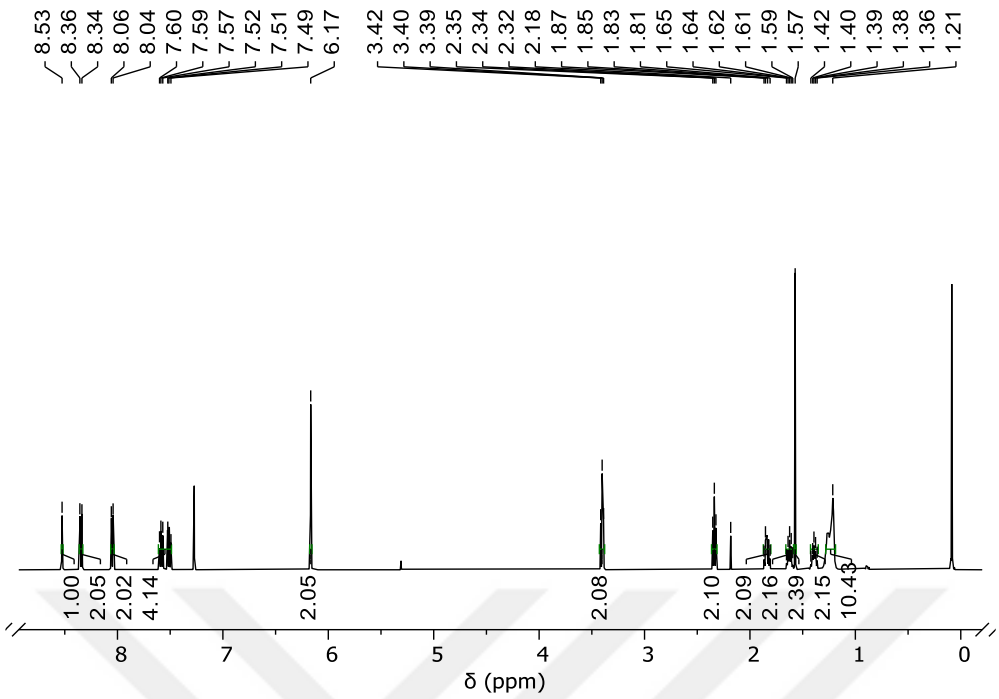

Figure 2.10 : ^{1}H NMR spectrum of Ant-Br in $CDCl_3$ at 25 °C.

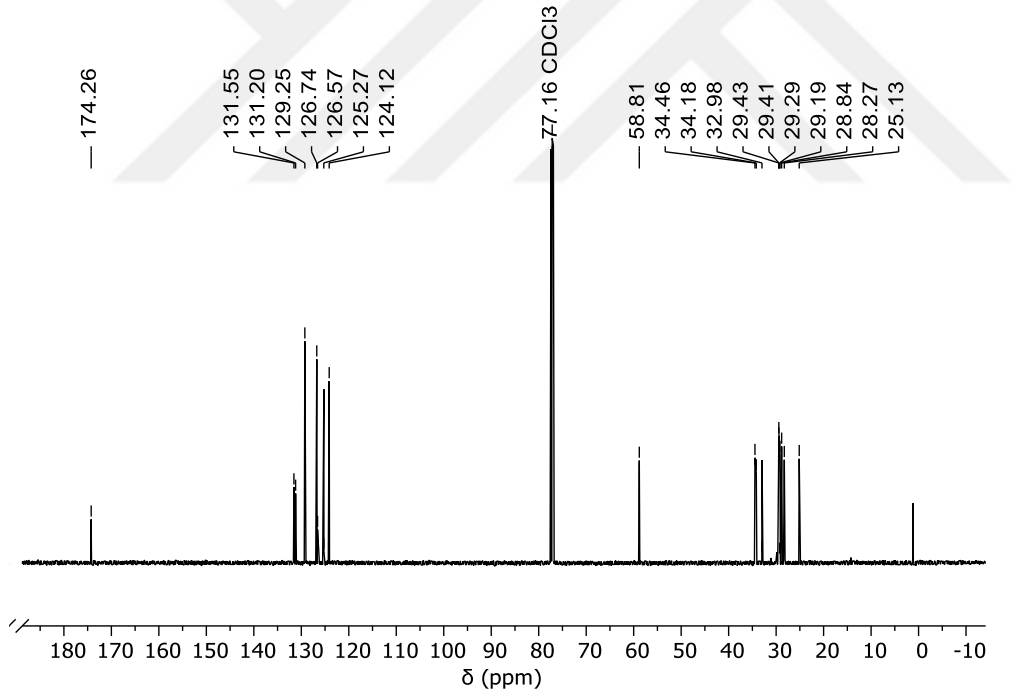

Figure 2.11 : ^{13}C NMR spectrum of Ant-Br in $CDCl_3$ at 25 °C.

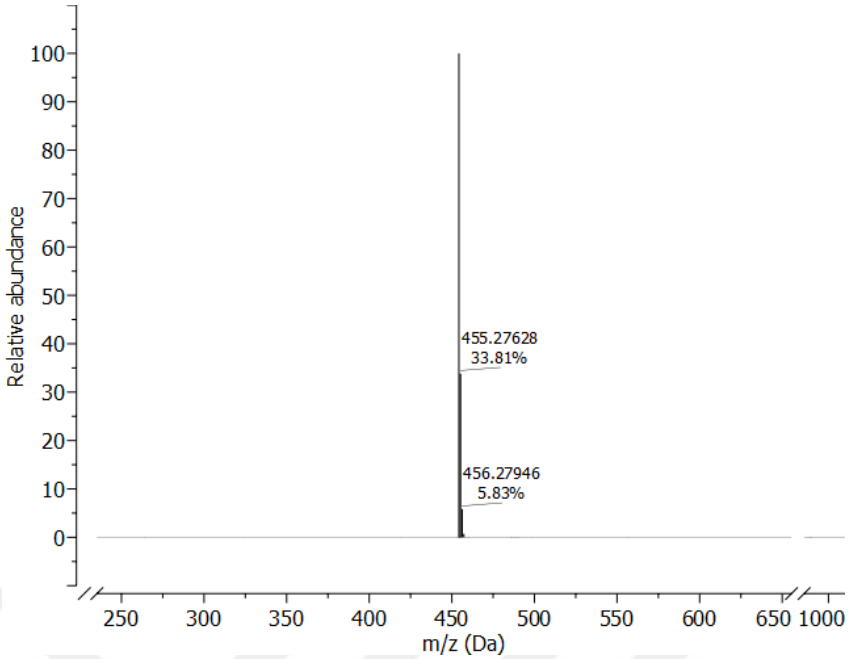

Figure 2.12 : HR-ESIMS of Ant-Br.

2.3.4 Synthesis of Pyridinium Bromide Salts of Calix[4]pyrrole (1-Br) and Anthracene (Ant-Py).

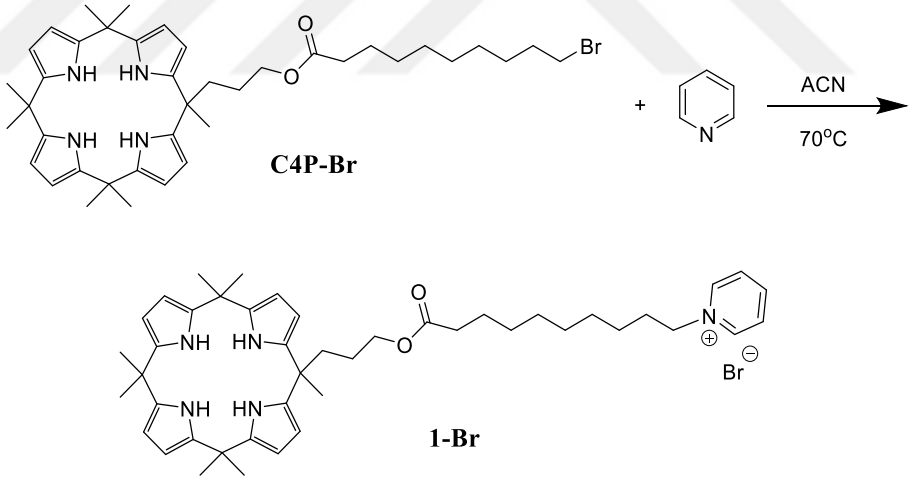

To a solution of bromo calix[4]pyrrole (400 mg, 566.71 µmol) in 15 ml of dry acetonitrile, an excessive amount of dry pyridine (2 mL) was added dropwise while nitrogen gas was passing through the schlenk flask. After 43 hours, the concentrated reaction mixture was purified by precipitation in diethyl ether and the yellowish solid was further dried under vacuum (400 mg, Yield: 89.92 %). M.p. decomposes over 175-180 °C. ^{1}H NMR (500 MHz, $CDCl_3$) δ = 10.60 (s, 4H), 7.26 (s, 2H), 7.21 (s, 1H), 6.55 (s, 2H), 5.49 (s, 8H), 4.14 (s, 2H), 3.73 (s, 2H), 2.36 (s, 4H), 1.76 (s, 11H), 1.58 (s,

19H), 1.26 (s, 10H). ^{13}C NMR (126 MHz, $CDCl_3$) δ = 174.1, 145.6, 142.6, 140.6, 127.3, 101.1, 38.3, 35.1, 35.0, 28.7, 28.6, 28.3, 24.9.

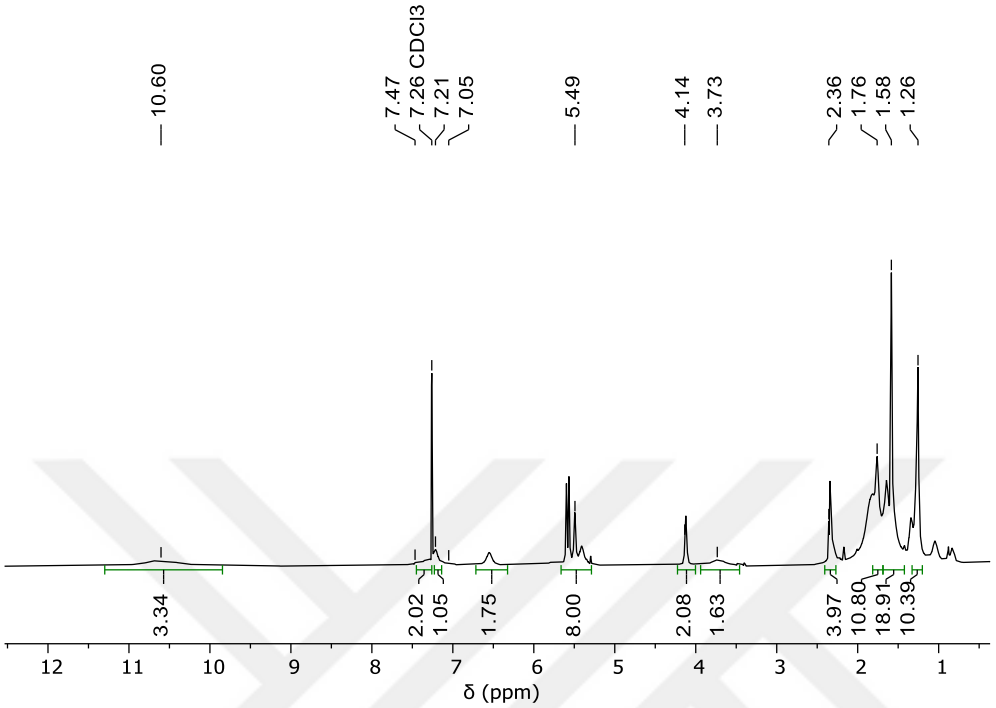

Figure 2.13 : ^{1}H NMR spectrum of 1-Br in $CDCl_3$ at 25 °C.

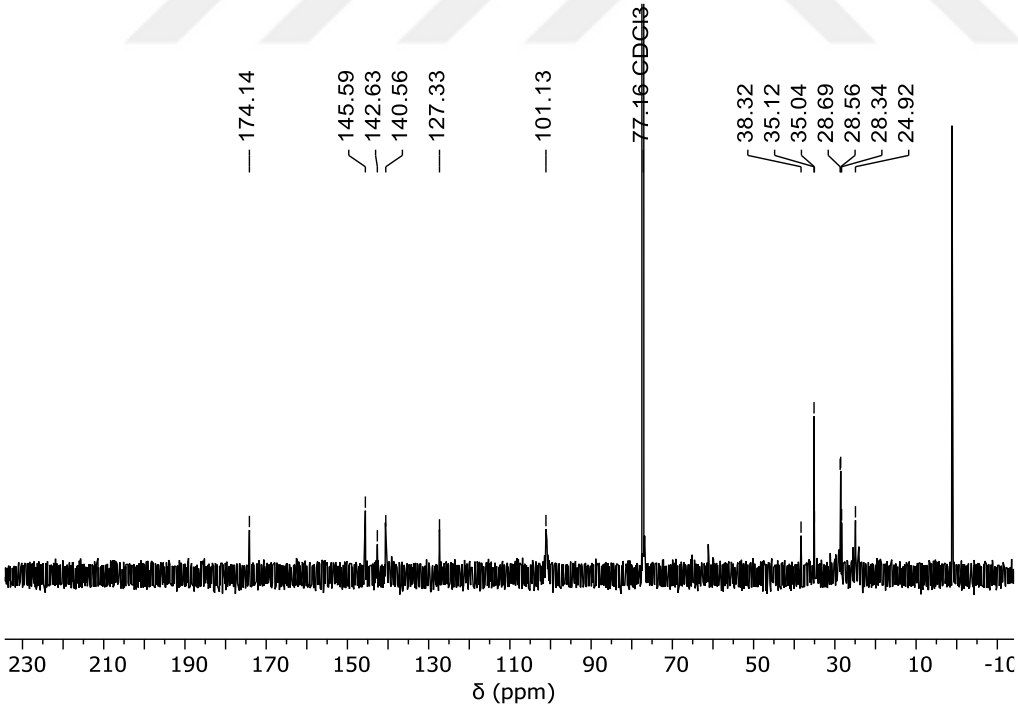

Figure 2.14 : ^{13}C NMR of 1-Br in $CDCl_3$ at 25 °C.

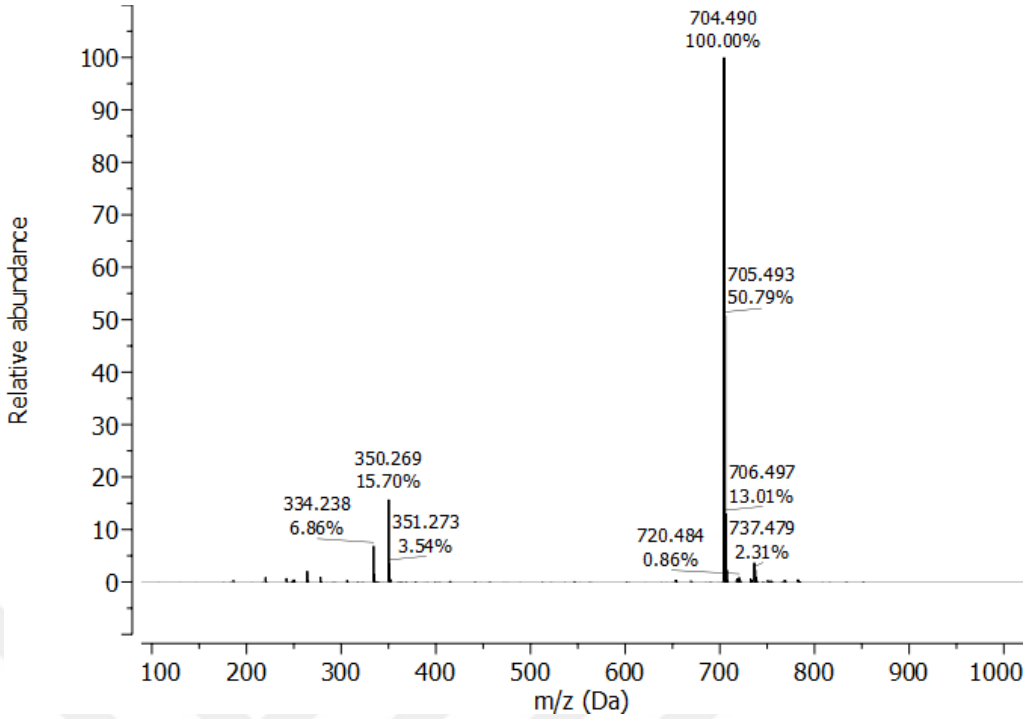

Figure 2.15 : Pos-HR-ESIMS of 1-Br.

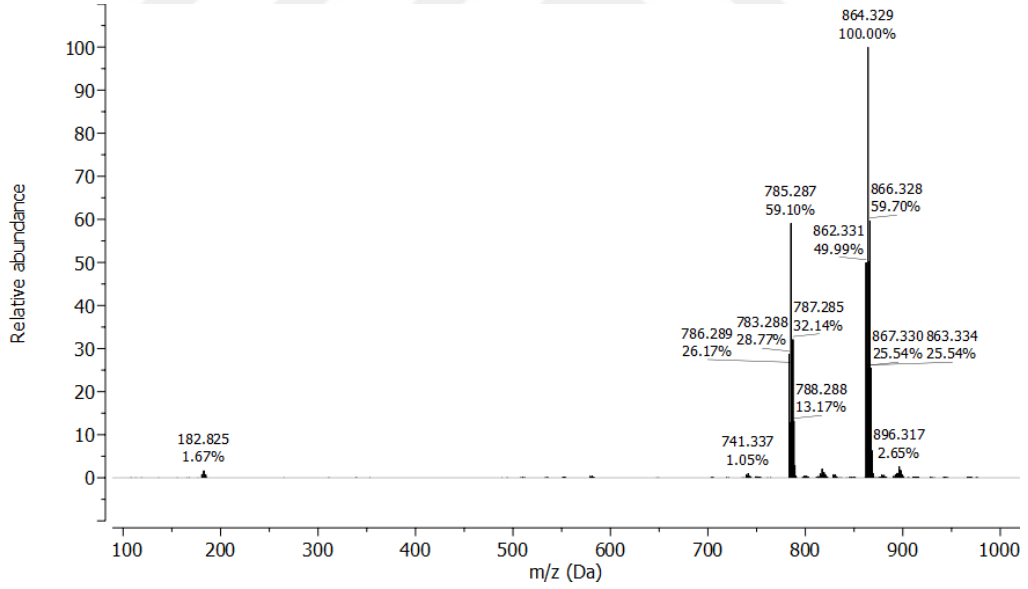

Figure 2.16 : Neg-HR-ESIMS of C4P-Py.

The same procedure was applied to the synthesis of pyridinium salt of anthracene (436 mg, Yield: 92.87 %) using **Ant-Br** (400 mg, 878.28 µmol) and an excessive amount of pyridine (2 mL) as the starting materials in the presence of dry acetonitrile. M.p. 124-125 °C. ^{1}H NMR (500 MHz, $CDCl_3$) δ = 9.41 (d, J = 6.0 Hz, 2H), 8.52 (s, 1H), 8.47 – 8.43 (m, 1H), 8.33 (d, J = 8.8 Hz, 2H), 8.07 (t, J = 6.7 Hz, 2H), 8.04 (d, J = 8.5 Hz, 2H), 7.60 – 7.55 (m, 2H), 7.50 (t, J = 7.4 Hz, 2H), 6.15 (d, J = 1.5 Hz, 2H), 4.99

(t, J = 7.3 Hz, 2H), 2.31 (t, J = 7.4 Hz, 2H), 1.99 (q, J = 7.6 Hz, 2H), 1.59 (p, J = 7.3 Hz, 3H). ^{13}C NMR (126 MHz, $CDCl_3$) δ = 174.2, 145.2, 131.5, 131.1, 129.2, 128.4, 126.7, 126.5, 125.2, 124.1, 62.2, 58.8, 34.4, 32.0, 29.2, 29.2, 29.1, 29.0, 29.0, 26.0, 25.0.

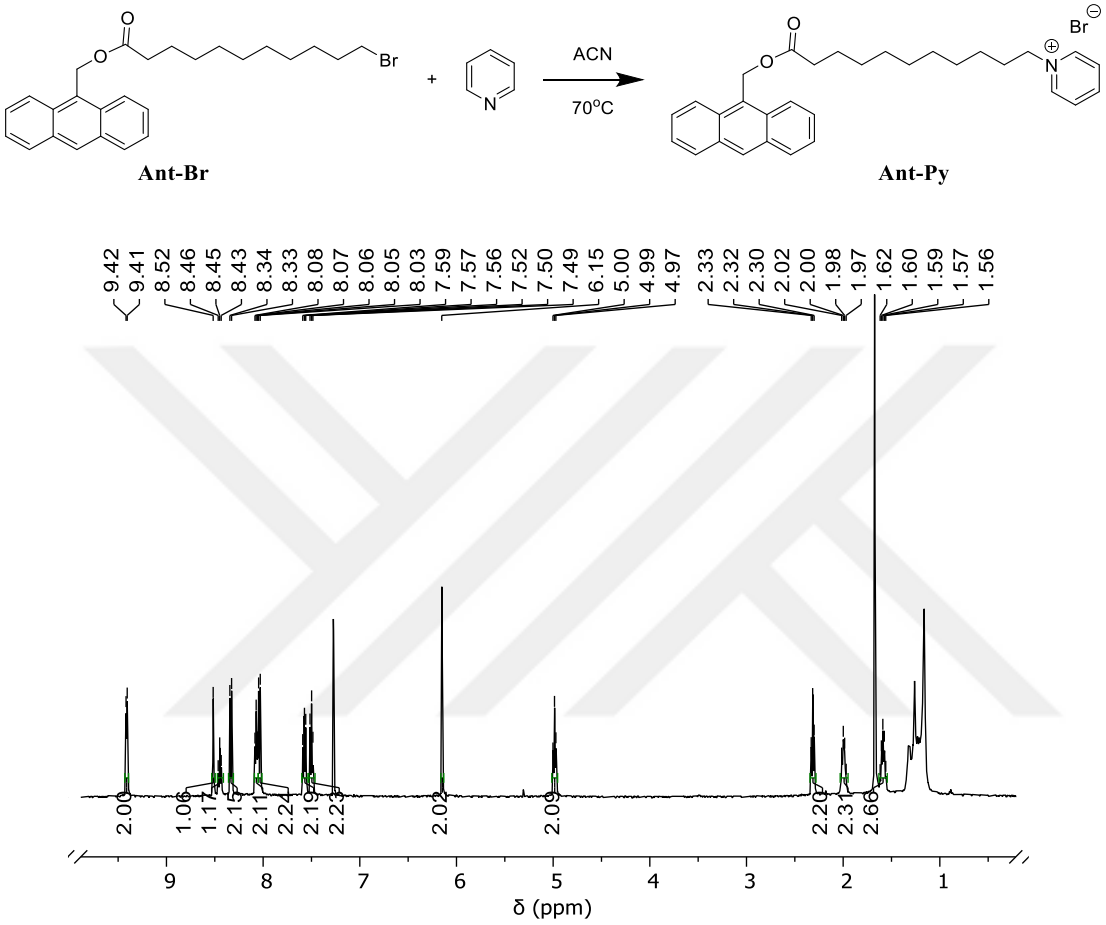

Figure 2.17 : ^{1}H NMR of Ant-Py in $CDCl_3$ at 25 °C.

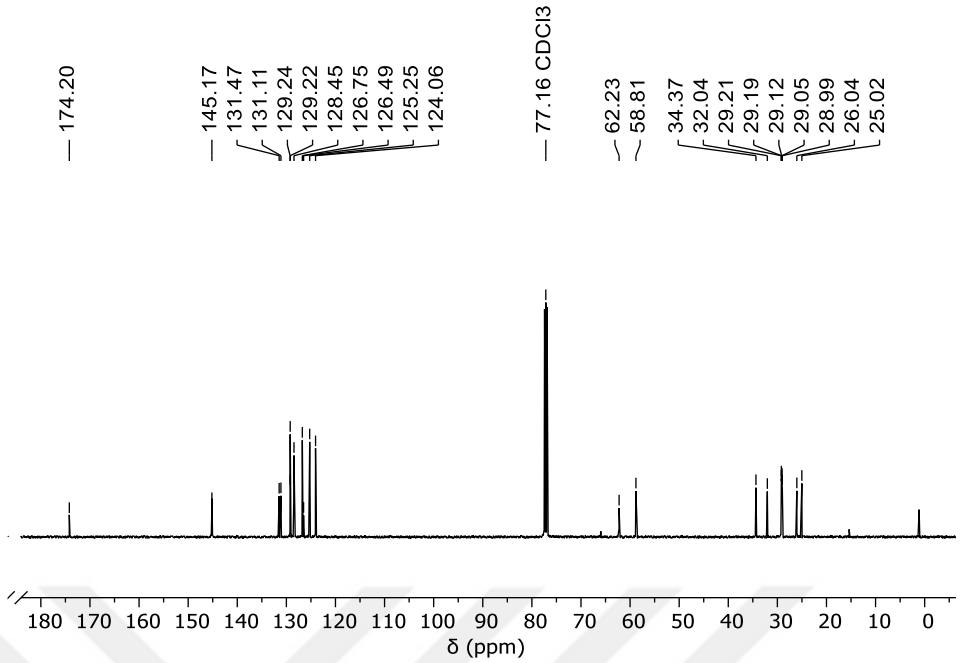

Figure 2.18 : ^{13}C NMR of Ant-Py in $CDCl_3$ at 25 °C.

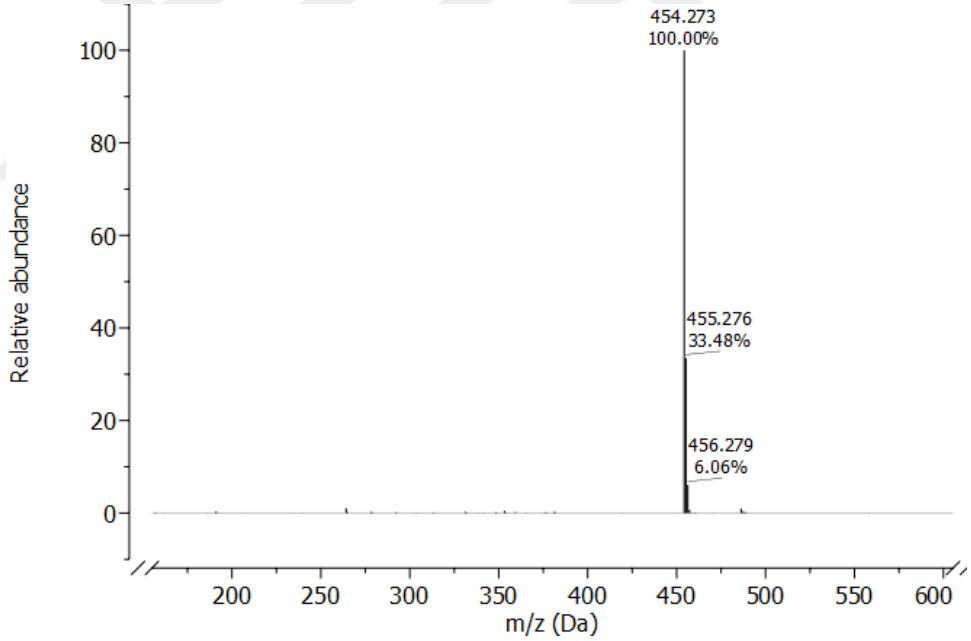

Figure 2.19 : HR-ESIMS of Ant-Py.

2.3.5 Synthesis of Pyridinium Hexafluorophosphate of Calix[4]pyrrole (1-PF6).

5g of Amberlyst A-26 hydroxide was loaded in a column and treated with 1 % KPF_6 multiple times until the pH became constant at around 3. Afterward, pyridinium bromide of calix[4]pyrrole (100 mg) was dissolved in approximately 30 ml of MeOH and was added to the Amberlyst A-26 PF_6-loaded column. The **1-Br** prepared solution

in MeOH was passed through the column several times. Finally, the obtained solution was evaporated and further dried in a vacuum oven at 40 °C.

3. RESULTS AND DISCUSSION

3.1 C4P-PEG and DOX complexation

The initial step to shed light on the complexation characteristics of **C4P-PEG** and DOX·HCl, involved using ^{1}H NMR analysis in DMSO-d_6. For this purpose, **C4P** was also used as a control compound to gain a deeper understanding of the fundamental chemical shifts that we were expecting, given that both **C4P** and **C4P-PEG** contain pyrrole rings.

Therefore, when **C4P** and **C4P-PEG** were treated with an equimolar of DOX, the significant chemical shifts related to the host-guest complexation between **C4P** and chloride anion of DOX were observed (Figure 3.1). Initially, pyrrole-NH resonance signals of both anion-free forms of the control compound **C4P** and **C4P-PEG** were observed at 9.24 ppm. These peaks exhibited downfield shifts after treatment with equimolar DOX and were observed around 10.96 ppm in the form of broad resonance signals.

Similarly, but conversely, pyrrole–CH peaks were found to be upfield shifted from 5.67 to 5.49 ppm after treatment of both the control **C4P** and **C4P-PEG** with DOX. These upper and lower field chemical shift changes are typical of what is observed when a calix[4]pyrrole molecule interacts with an anion, and show the successful complexation of control compound **C4P** with counter chloride anion of DOX in DMSO. It also indicates that **C4P-PEG** can form the same complex with chloride anion in the presence of its PEGylated version.

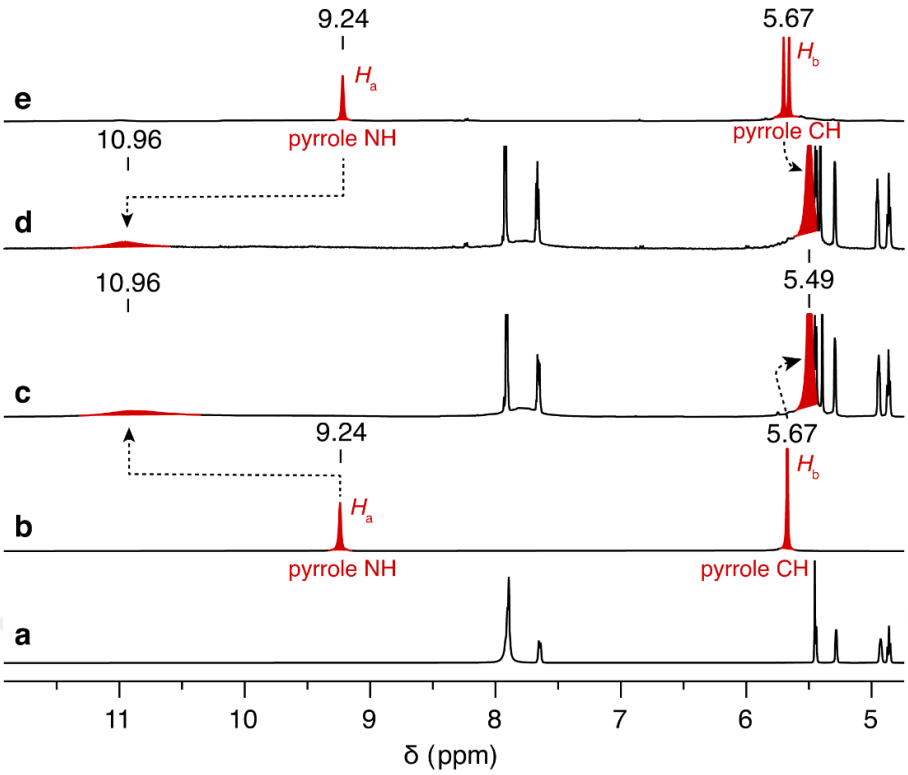

Figure 3.1 : (a) DOX·HCl (b) C4P, (c) C4P +DOX, (d) C4P-PEG+DOX and (e) C4P-PEG in DMSO-d_6 and corresponding N-H and C-H pyrrole chemical shifts changes.

Another characterization technique that was used to confirm DOX and **C4P** complexation was using Fourier Transform Infrared (FT-IR) spectroscopy (Figure 3.2). Accordingly, the peaks corresponding to the pyrrole N–H bond stretching bands of **C4P** and **C4P-PEG** at 3436 (3416 in the case of **C4P**) cm^{-1} merged with DOX bands and observed as a broad band between 3652 and 3129 cm^{-1} upon interaction with DOX. Additionally, the bands representing the pyrrole C–NH stretching perturbations of **C4P-PEG** and **C4P** shifted from 1229 to 1184 cm^{-1} for both molecules.

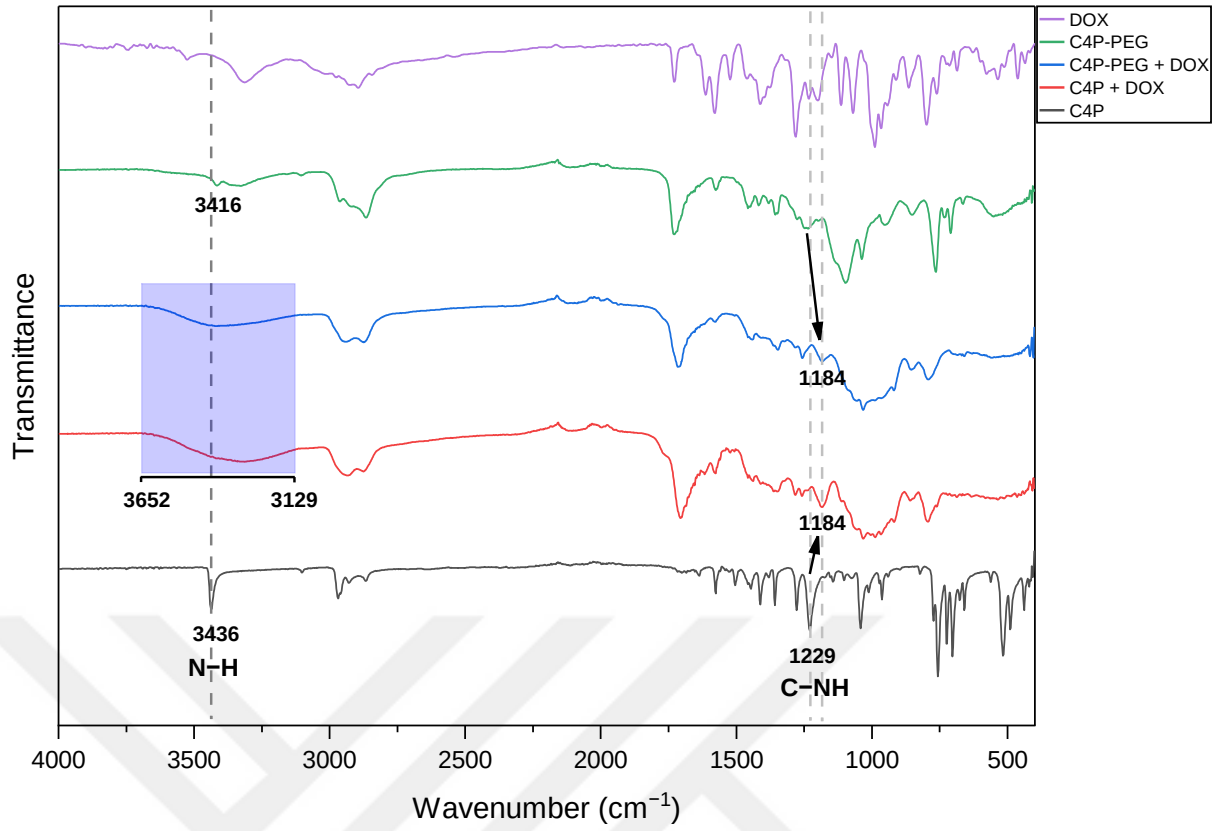

Figure 3.2 : Stacked FTIR spectra of DOX, C4P, C4P + DOX, C4P-PEG and C4P-PEG + DOX.

The results from FTIR were in agreement with the ^{1}H NMR analysis in a way that confirms **C4P-PEG** and DOX·HCl can successfully form a complex with the chloride counter anion of DOX in DMSO.

3.2 Micelle Formation

In order to examine the capability of **C4P-PEG** in forming larger aggregates, a couple of methods were utilized to acquire further confirmation.

The first method was performing ^{1}H NMR in D_2O where only the PEG segment of **C4P-PEG** was visible in the spectrum which is an indication of **C4P** being effectively shielded in an aqueous environment where the hydrophobic cavity of **C4P** remains protected (Figure 3.3). Moreover, it strongly corroborates the formation of larger-order aggregates.

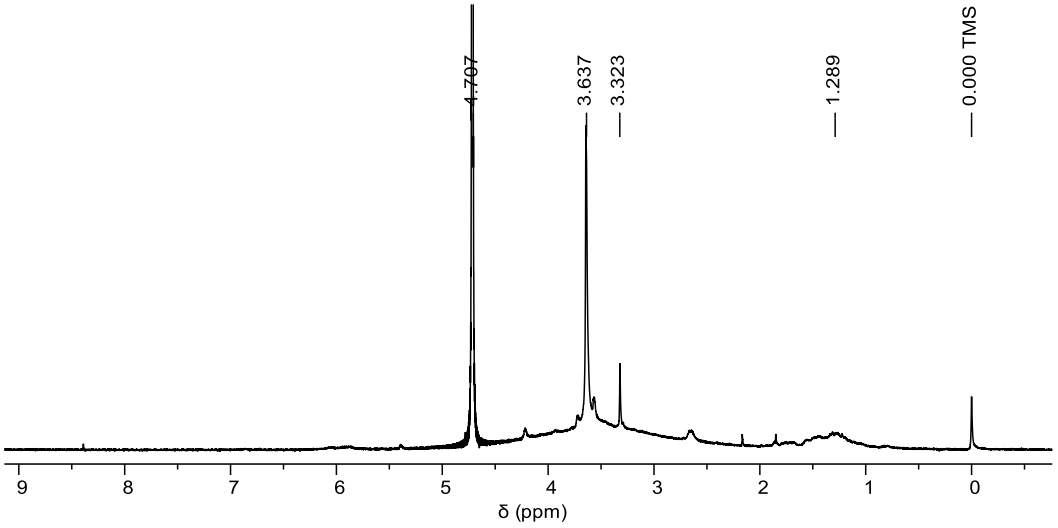

Figure 3.3 : ^{1}H NMR spectrum of C4P-PEG in D_2O.

The second method was using DLS in order to obtain further information regarding the size and size distribution of the aggregates and the CMC value (Figure 3.4).

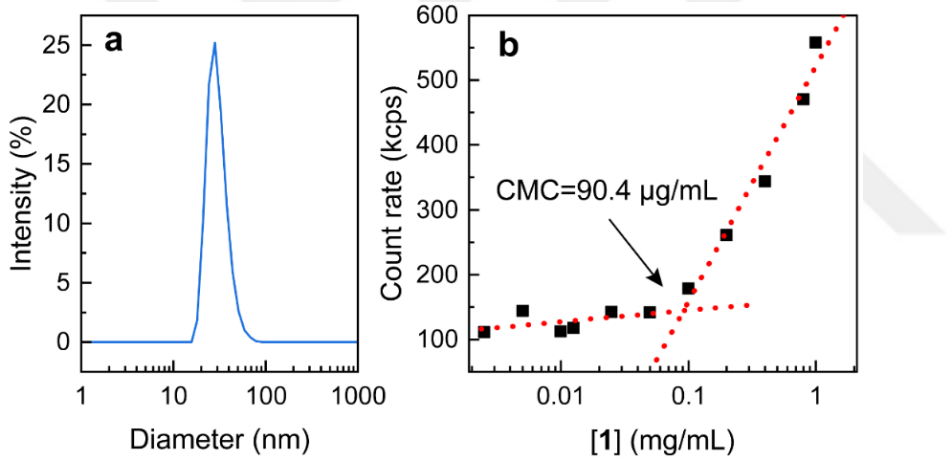

Figure 3.4 : (a) Size distribution of C4P-PEG and (b) Critical micelle concentration of C4P-PEG determined via concentration-dependent DLS measurements.

For this purpose, the nanoprecipitation method was used for preparing the self-assembled **C4P-PEG**s. Summarily, **C4P-PEG** (5 mg) was dissolved in DMSO (0.6 mL) and the obtained solution was added dropwise into ultra pure water (4.4 mL) using a syringe pump at a rate of 0.5 mL/h. Next, DMSO was removed by means of the dialysis method. Accordingly, the hydrodynamic size of micelles obtained from **C4P-PEG** was located at 27.71 ± 1.22 nm with a narrow size distribution of 0.32 ± 0.06 nm. Moreover, the CMC of amphiphilic molecules can be defined as the specific concentration at which amphiphile molecules aggregate to form micelles in solution. By finding the intersection point in the graph of count rate versus concentration, the CMC value was determined to be 90.4 µg/mL.

Another method that was used to confirm the formation of larger aggregates was controlling the Tyndal effect. The Tyndall Effect, a widely recognized optical phenomenon, provides solid evidence of a substantial number of nanoparticles being present in the **C4P-PEG** solution (Figure 3.5). This phenomenon, marked by the scattering of light, serves as direct evidence of the presence of these nanoparticles, providing support for their existence and suggesting the creation of micelles.

Figure 3.5 : Tyndall effect (right: only ultra-pure water. Left: aqueous solution of C4P-PEG (1.67 mg/mL).

The confirmation of the spherical morphology of the micellar system in our synthesized structure was reaffirmed through TEM analysis. When analyzing the sample containing **C4P-PEG** and water, we observed spherical structures of **C4P-PEG** with an average diameter of 29.17 ± 0.70 (Figure 3.6).

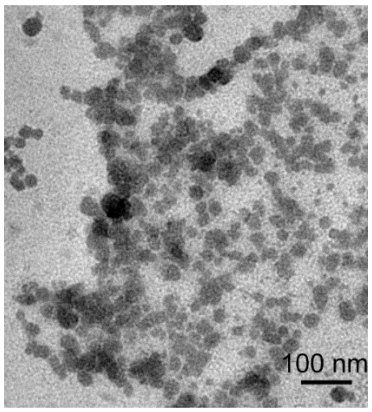

Figure 3.6 : TEM image of C4P-PEG micelles.

3.3 Drug Loading and Release

In order to investigate whether **C4P-PEG** is capable of being effectively used as a drug carrier and its release behavior under different pH conditions (Figure 3.7), the first step was using the nanoprecipitation method, which was previously used for

preparing drug-free micelles, to prepare the doxorubicin-loaded micelles. For this purpose, 5 mg of **C4P-PEG** and 2.5 mg of DOX were used. The excessive amount of DOX was removed utilizing dialysis against ultra-pure water which afforded drug-loaded micelles and will be referred to as **C4P-PEG-DOX**.

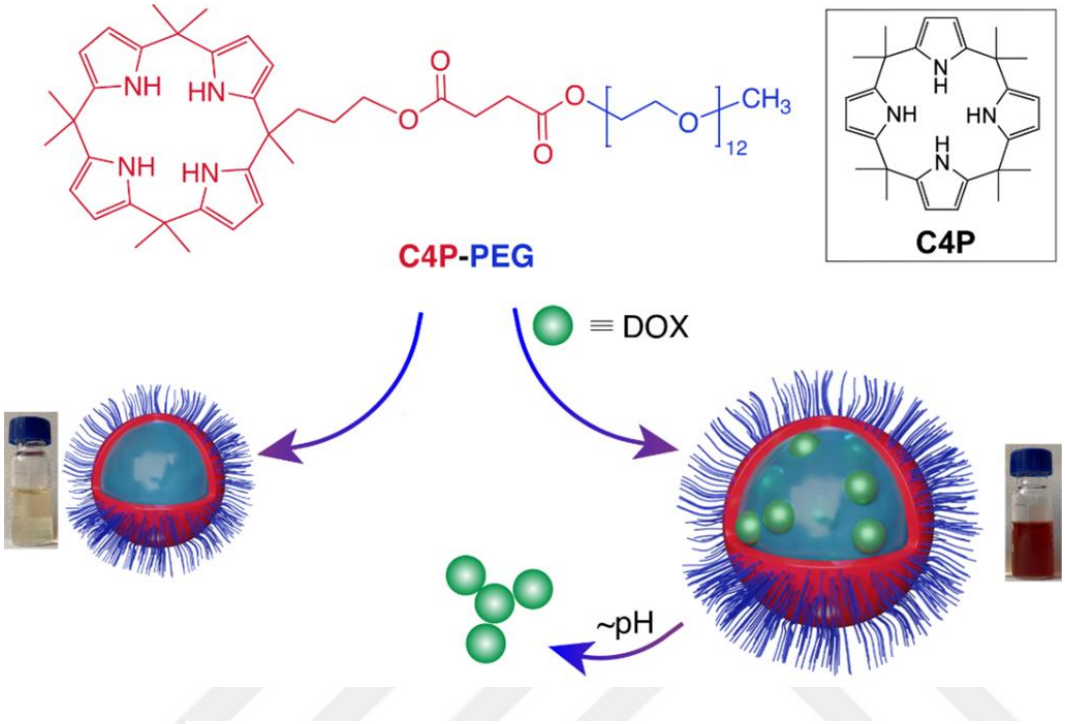

Figure 3.7 : Schematic representation of C4P-PEG micelle formation and DOX loading and subsequent release due to pH responsiveness.

DLS method was again utilized to gain information regarding the size and distribution of drug-loaded micelles and the CMC value (Figure 3.8). Accordingly, **C4P-PEG-DOX** possesses an average hydrodynamic size centered at 54.62 ± 0.62 nm with a narrow size distribution of 0.13 ± 0.07 nm.

Moreover, for determination of the CMC of drug-loaded micelles, a concentration-dependent DLS analysis was again performed which revealed a CMC value of 184.2 µg/mL showing a higher value in comparison to the unloaded micelles.

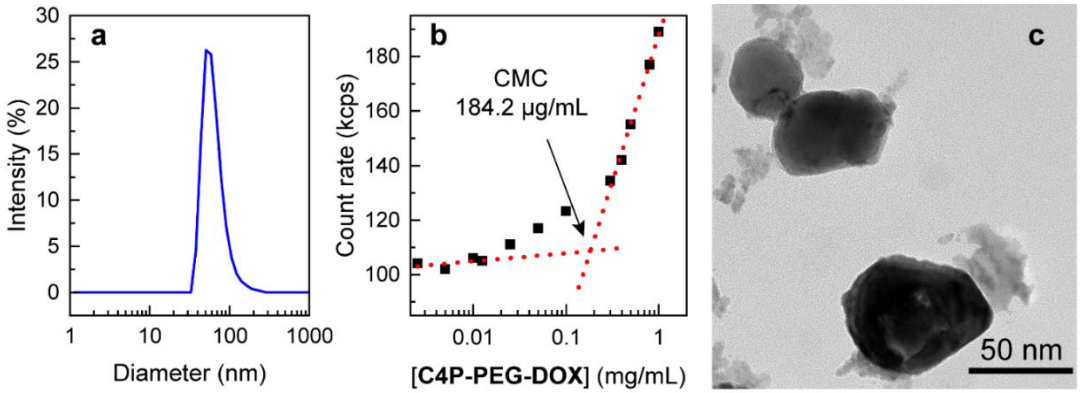

Figure 3.8 : (a) Size distribution of C4P-PEG-DOX (b) CMC of C4P-PEG-DOX (c) TEM image of C4P-PEG-DOX.

Further support was provided through TEM imaging where spheroidal micelles with an average diameter of about 51.7 nm in ultra-pure water were detected, although it is necessary to mention that the small difference in diameter between TEM and DLS results was attributed to the shrinkage of micelles during the drying stage of TEM sample preparation.

The next step was calculating Drug Loading Capacity (DLC) and Encapsulation Efficiency (EE) properties. EE and DLC profiles of **C4P-PEG** were studied using UV-vis measurements before and after disassembling the **C4P-PEG-DOX** micelles with DMSO, respectively (Figure 3.9).

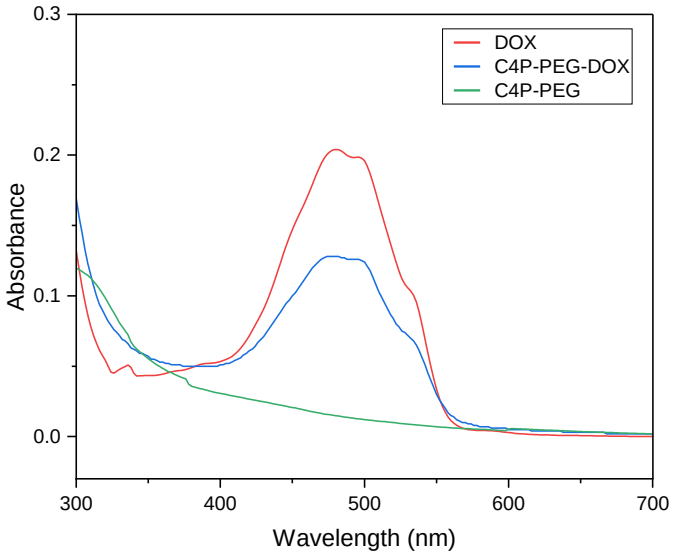

Figure 3.9 : UV-Vis spectra of DOX, unloaded C4P-PEG micelles and loaded C4P-PEG micelles.

Quantification of supernatants via calibration curve of DOX (Figure 3.10) resulted in ca. 18.63 ± 0.55 % DLC and ca. 36.89 ± 1.62 % EE which were comparable with similar supramolecular drug carrier systems reported earlier.

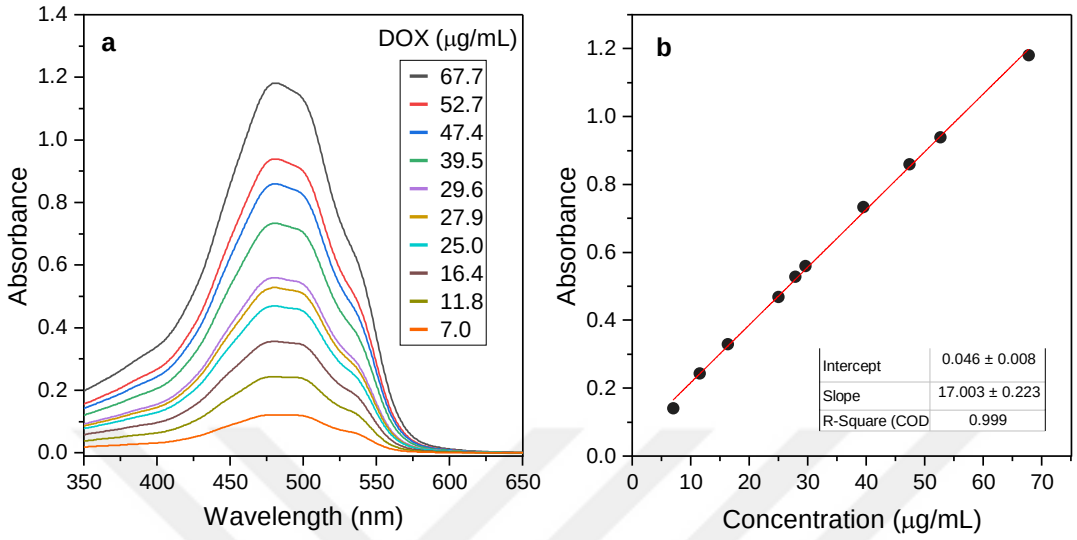

Figure 3.10 : (a) UV-Vis spectra of DOX in DMSO at different concentrations and (b) the corresponding calibration curve generated from the absorbance values at 593 nm.

The equations below were used to calculate the DLC and EE percentages:

$$\% \text{ DLC} = \frac{\text{weight of loaded drug}}{\text{weight of micelle}} \times 100 \qquad (3.1)$$

$$\% \text{ EE} = \frac{\text{weight of DOX in micelles}}{\text{weight of DOX in feed}} \times 100 \qquad (3.2)$$

For the in-vitro drug release assay of **C4P-PEG-DOX**, a time-dependent UV-Vis analysis was conducted and 1 mL of sample solution was taken into a clipped dialysis bag (MWCO: 3.5 kDa) and was immersed in a beaker containing 30 mL of either phosphate-buffered saline solution (PBS, pH 7.4) or acidic buffer solution (pH 5.5) under sink conditions at 37 °C. Then the beaker was transferred into an orbital shaker. 0.5 mL of samples were drawn from the outer medium at specific time intervals (0.5, 1, 2, 3, 4, 5, 6, 7, 24, 32, 48, 72, 96, and 120 h) and were replaced with fresh buffer solution (Figure 3.11). Accordingly, the cumulative release behavior of micelles at two different pH values (5.5 and 7.4) with no initial burst release is shown in the figure below. The UV-vis spectra show a favorable drug release attitude of **C4P-PEG-DOX** micelles and reveals that while the cumulative release of DOX was 64 % after 24 h under an acidic environment, it was found to be 57 % in the case of slightly alkaline condition. Drug release percentage of **C4P-PEG-DOX** approaches 82 and 68 % after

120 h under acidic and basic conditions, respectively, and emphasizes the stability and control over release kinetic along extended periods. The favorable drug release behavior under weakly acidic conditions (pH 5.5) may be attributed to the destruction of the host-guest attraction between the calix[4]pyrrole units of **C4P-PEG** and chloride counter anion of DOX molecule and the alteration of the hydrophilic/hydrophobic balance of micelles.

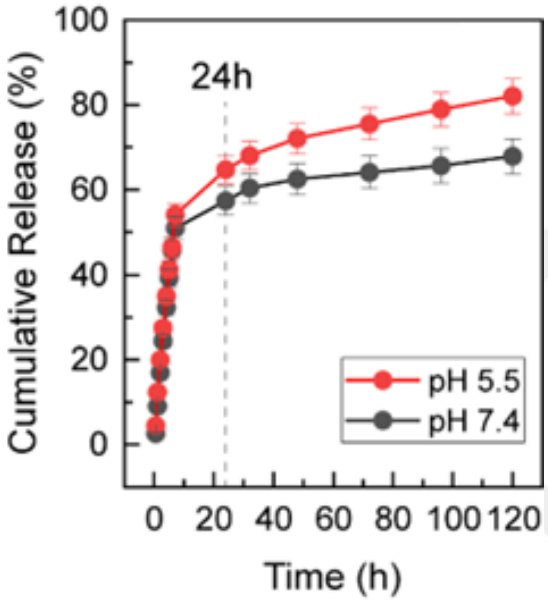

Figure 3.11 : Cumulative release profiles of DOX-loaded micelles in phosphate-buffered saline solution (pH 7.4) and acidic buffer solution (pH 5.5).

3.4 Poly-Pseudorotaxane Formation

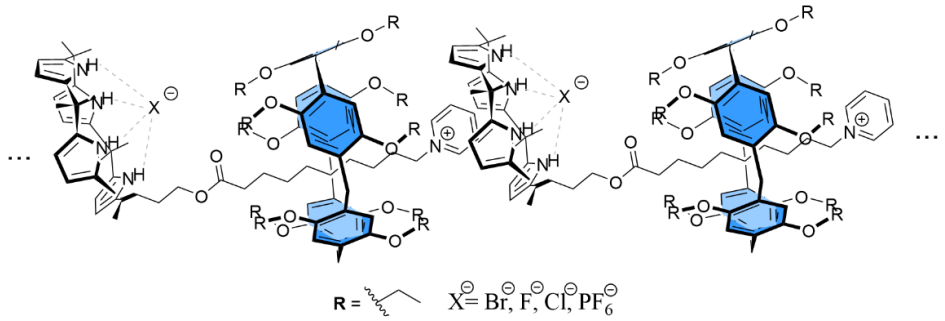

Figure 3.12 : Structure of poly-pseudorotaxane formed via ion-pair recognition of calix[4]pyrrole and successful thread of perethylayted pillar[5]arene.

To provide evidence for the suggested poly-pseudorotaxane structure shown above (Figure 3.12), ^{1}H NMR spectroscopy was the primary method of analysis. **C4P** has been known to be capable of acquiring cone conformation upon interacting with anions which consequently allows cations to interact with its electron bowl formed by the similarly oriented pyrrole units. This concept was manifested as we compared the bromo calix[4]pyrrole (**C4P-Br**) ^{1}H NMR result with pyridinium bromide of calix[4]pyrrole (**1-Br**) (Figure 3.13). Accordingly, the interaction between pyrrolic N-H and Br^{-} through hydrogen bonding was detected by the broadened and shifted peaks of pyrrolic N-H to downfield (from 7.05 to 10.61 ppm) and pyrrolic C-H to upfield (5.90 to 5.57 ppm). Similar changes in chemical shifts have been reported in previous literature, consistent with the anion complexation of **C4P** [33]. Moreover, all the resonance signals were broadened and the peak corresponding to **−CH₂-Br** and **−CH₂OCO** were slightly shifted downfield (3.41 to 3.75 ppm and 3.95 to 4.13 ppm, respectively) in the case of **1-Br**. These results, suggested us the formation of an ion-pair complex and also the occurrence of supramolecular polymerization.

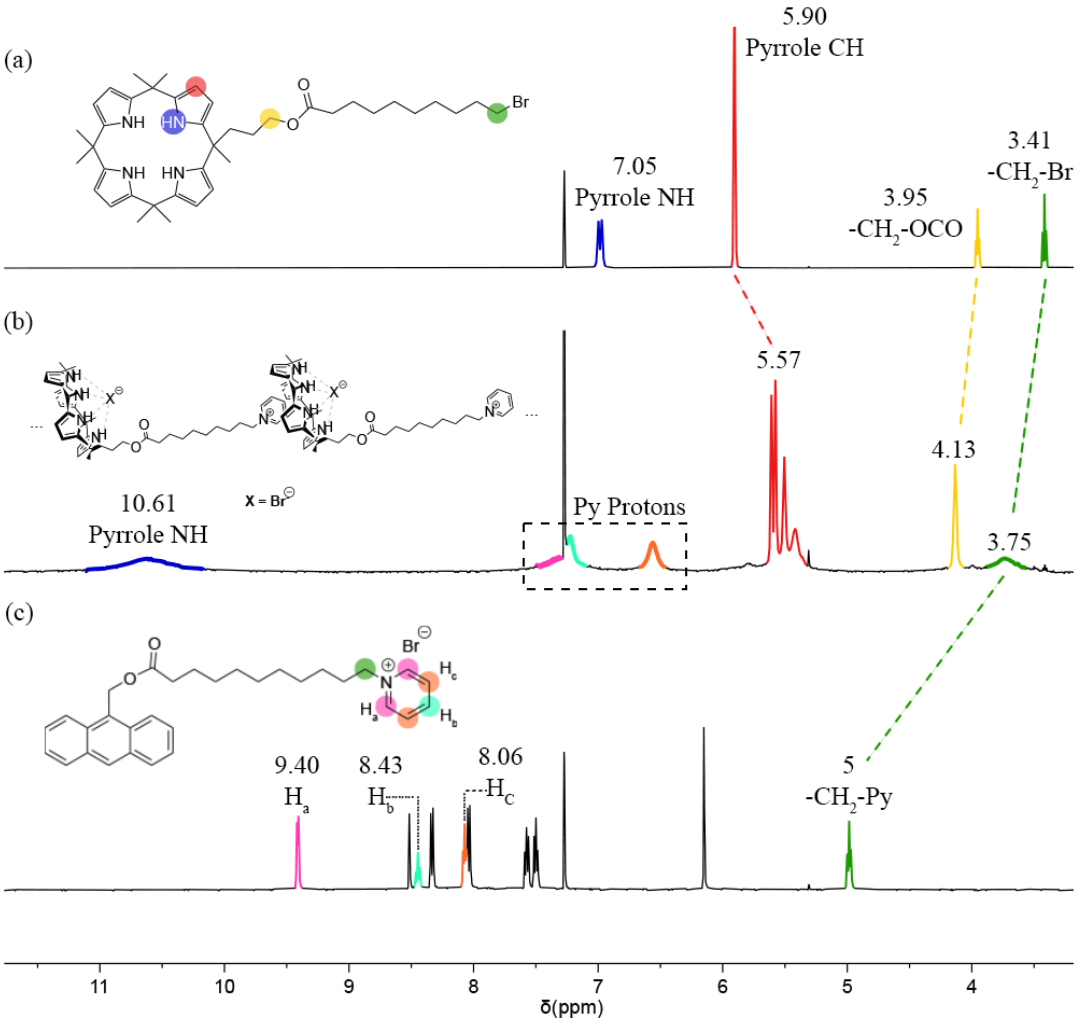

Figure 3.13 : Stacked ^{1}H NMR spectra of (a) C4P-Br, (b) 1-Br and (c) Ant-Py in $CDCl_3$ at 25 °C.

Due to the obstacles regarding the interpretation of ^{1}H NMR spectra as a result of the supramolecular polymerization, pyridinium salt of an anthracene derivative (**Ant-Py**) was synthesized as a model system. This approach allowed us to investigate non-covalent interactions and to understand the changes in chemical shifts more accurately with the absence of a supramolecular polymerization. As a result, **Py** protons that are typically detected between 8 to 10 ppm according to the **Ant-Py** ^{1}H NMR result, became broadened and showed an upfield shift in the case of **1-Br** due to the non-covalent interactions. The presence of **C4P** reveals another identifiable change in the 1-Br spectra that is related to the protons of the alkyl group being adjacent to the **Py** unit (**-CH2-Py**). While the pinpointed signal in the **Ant-Py** spectra is observed around 5 ppm, it noticeably shifted to the upfield as a broadened peak at 3.75 ppm in the spectrum of **1-Br** due to supramolecular polymerization. These observations suggest

that the synthesized supramolecular polymeric axle is obtained through the ion-pair recognition capability of **C4P** units present in the structure of **1-Br**.

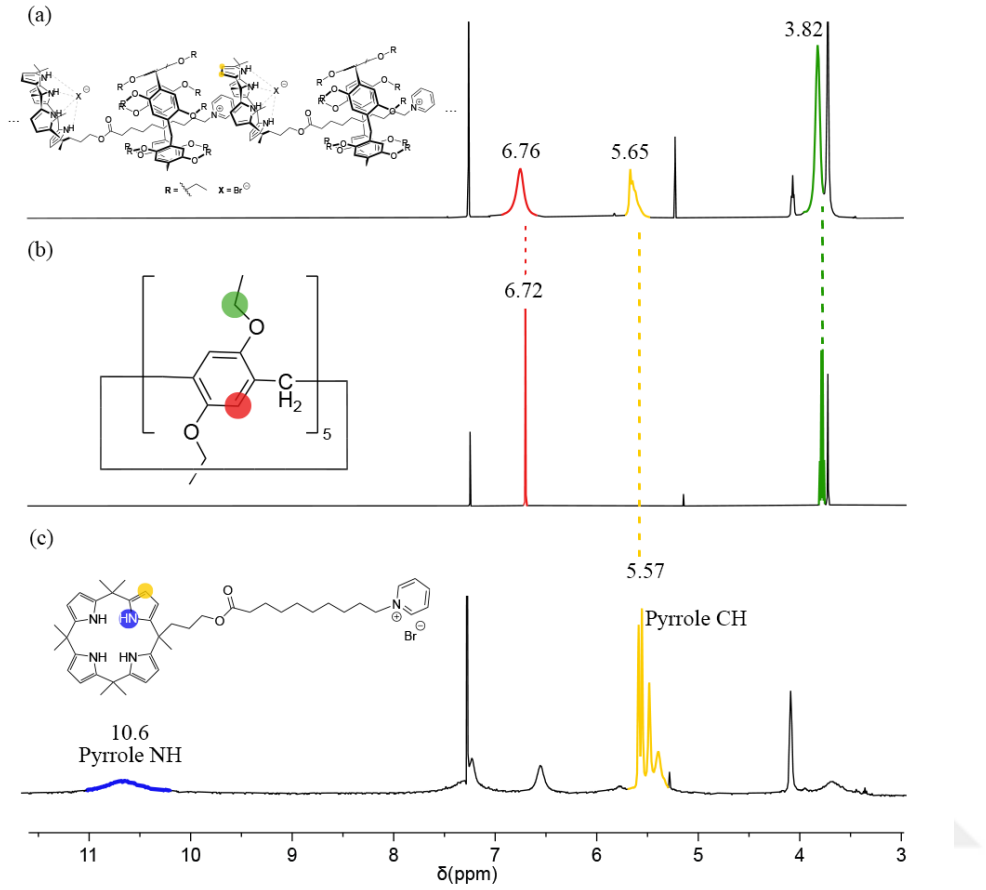

Figure 3.14 : Stacked ^{1}H NMR spectra of (a) 1-Br + EtP5A, **(**b) EtP5A and (c) 1-Br in $CDCl_3$ at 25 °C.

In the following step, we interacted one equivalent of **EtP5A** as the "wheel" of the poly-pseudorotaxane with **1-Br** (Figure 3.14). Due to robust complexation, the NMR signals of **Py** protons couldn't be pinpointed. However, we observed that the signals related to the hydrogens of the aromatic ring and the methylene of **EtP5A** were broadened and shifted slightly downfield (from 6.72 to 6.76 ppm, with a broadened peak at 3.82 ppm), respectively. Additionally, the peak corresponding to the pyrrole C-H of **C4P** displayed significant broadening due to strong complexation and shifted downfield (from 5.57 to 5.65 ppm), while the pyrrole N-H of **C4P** faded due to strong complexation.

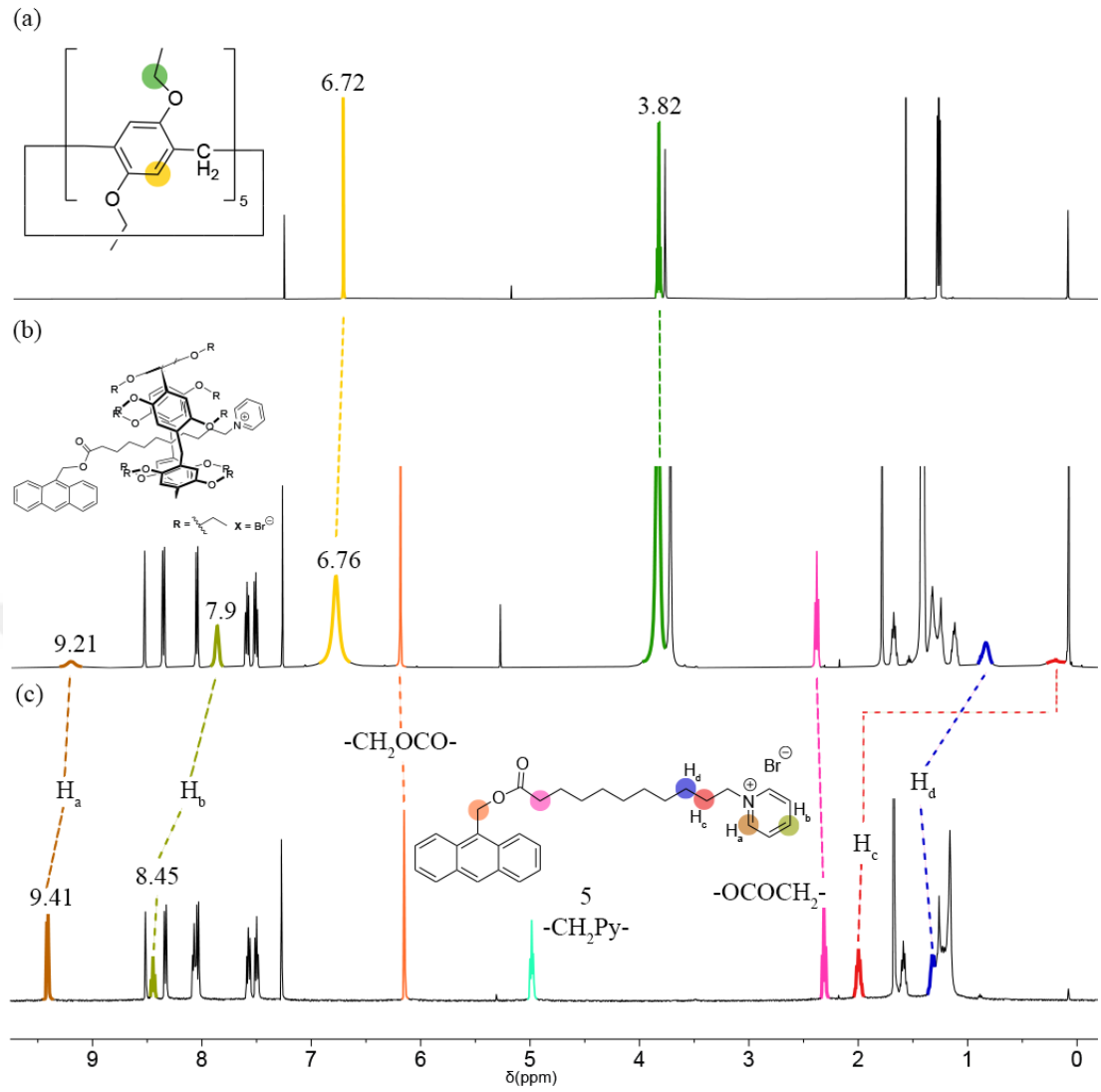

Figure 3.15 : Stacked ^{1}H NMR spectra of (a) EtP5A, (b) Ant-Py+EtP5A and (c) Ant-Py in $CDCl_3$ at 25 °C.

To gain a deeper understanding of these interactions, we simulated the same complexation using a mixture of **Ant-Py** and **EtP5A** in a (1:1) molar ratio (Figure 3.15). Upon interaction with threaded **EtP5A**, **Py** protons experienced a slight upfield shift in their signals. Specifically, the ortho and para protons exhibited transitions from 9.41 ppm to 9.21 ppm and 8.45 ppm to 7.9 ppm, respectively. Notably, the protons related to the alkyl groups adjacent to ester (**-CH2OCO-** and **-OCOCH2-**) showed no significant changes in the NMR spectra upon the addition of **EtP5A** which is a piece of evidence for supporting the proposed poly-pseudorotaxane structure. Additionally, a notable change was observed in the signal of the adjacent alkyl group (**-CH2-Py**) to the pyridinium unit (Figure 3.16). These protons exhibited a signal in the negative

region of the spectra at -0.85 ppm, contrary to the expected appearance at 4.97 ppm, indicating the presence of a magnetic anisotropic effect.

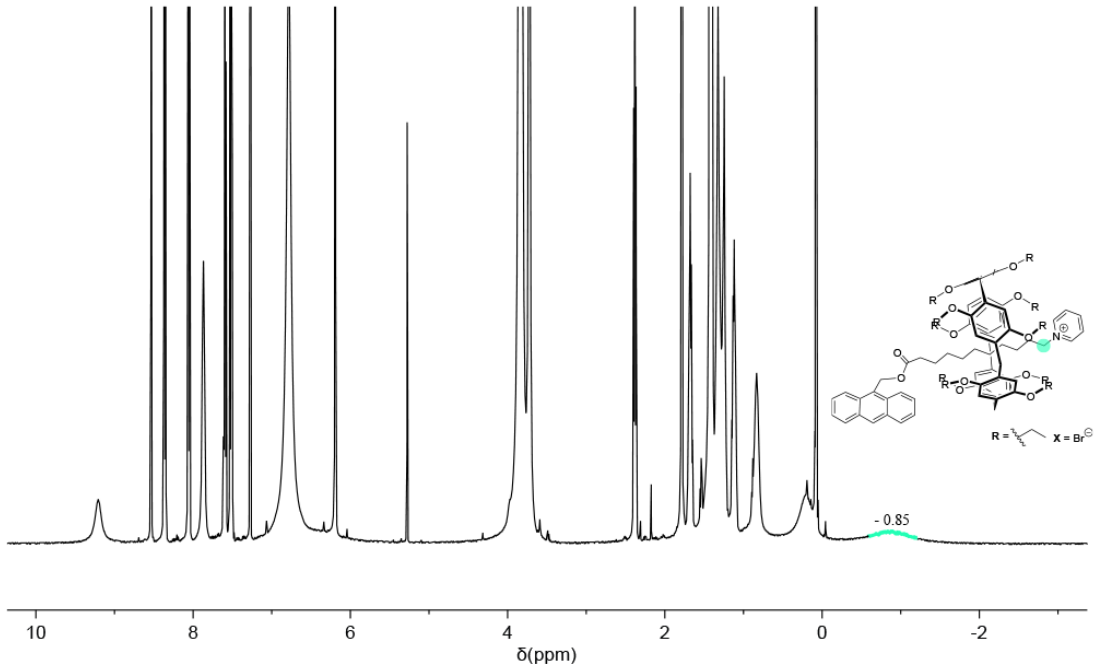

Figure 3.16 : ^{1}H NMR spectrum of Ant-Py+EtP5A in $CDCl_3$ at 25 °C.

This outcome was also in agreement with the NOESY NMR data (Figure 3.17); revealing clear correlations between the methylene group of **EtP5A** and neighboring protons of the **Py** unit.

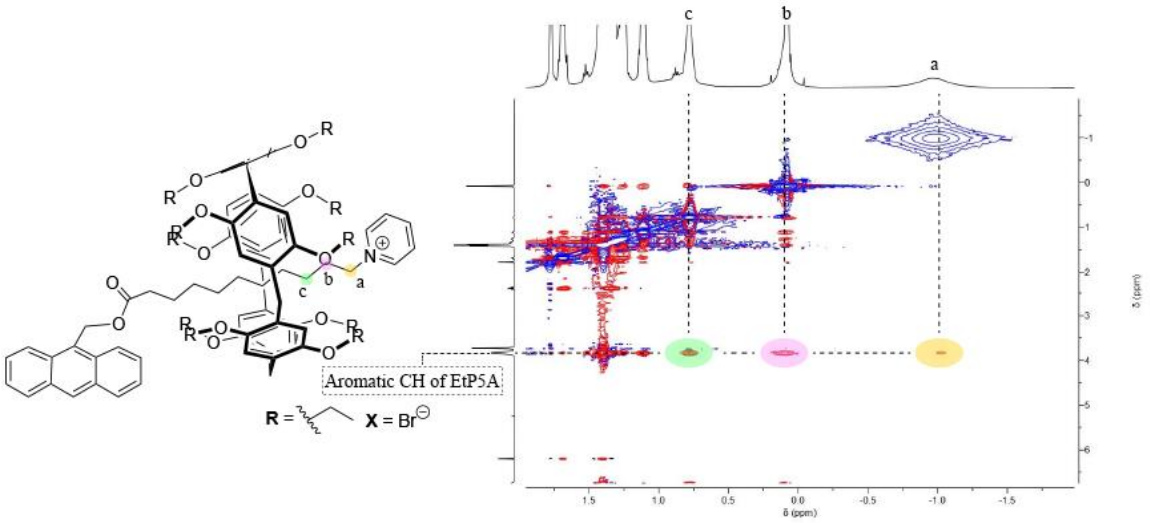

Figure 3.17 : NOESY spectrum of Ant-Py+EtP5A in $CDCl_3$ at 25 °C.

Upon addition of **C4P** to the **EtP5A** and **Ant-Py** mixture (1:1:1), we could see additional changes due to the ion pair recognition property of C4P resulting in the broadening and near-undetectability of the Py protons in the spectra (Figure 3.18).

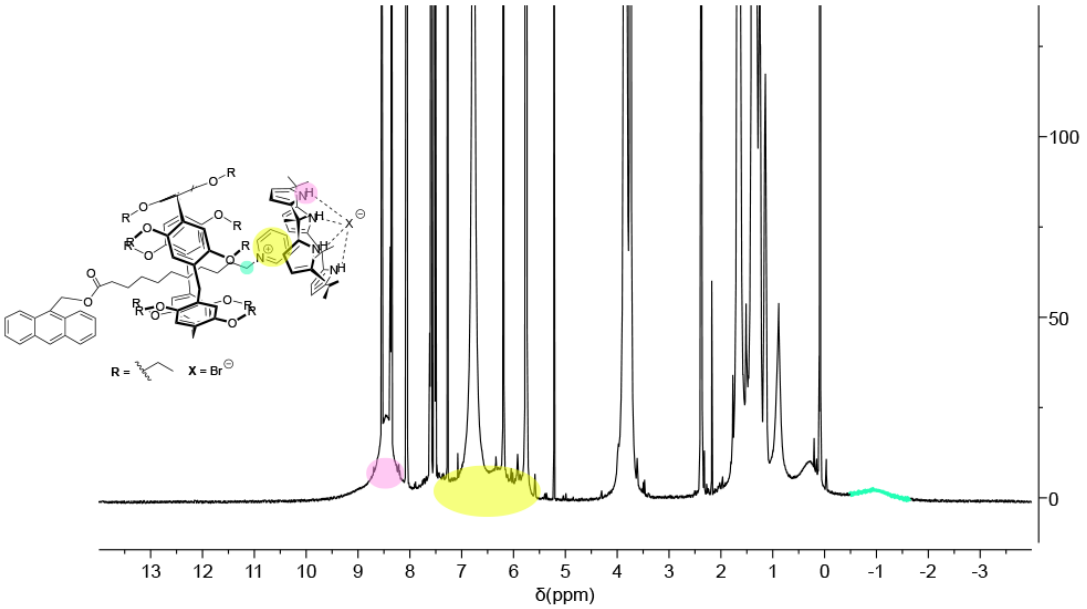

Figure 3.18 : ^{1}H NMR spectrum of equimolar Ant-Py + EtP5A + C4P in $CDCl_3$ at 25 °C.

Dilution NMR analysis provides valuable insights into the supramolecular polymerization process and poly-pseudorotaxane formation within our system (Figure 3.19). As the concentration of **1-Br + EtP5A** increases, the pyrrolic N-H peaks gradually shift from 8.3 ppm to 9.78 ppm, indicating continuous supramolecular polymerization. Additionally, evidence of poly-pseudorotaxane formation emerges concurrently, as observed through slight shifts in the pyrrole C-H signals of calix[4]pyrrole, which transition from 5.69 to 5.62 ppm. Moreover, at higher concentrations, the broadened peaks of aromatic protons of **EtP5A** indicate its sustained interaction within the poly-pseudorotaxane framework. These findings further reinforce the simultaneous occurrence of supramolecular polymerization and poly-pseudorotaxane formation, illuminating the dynamic processes within our system.

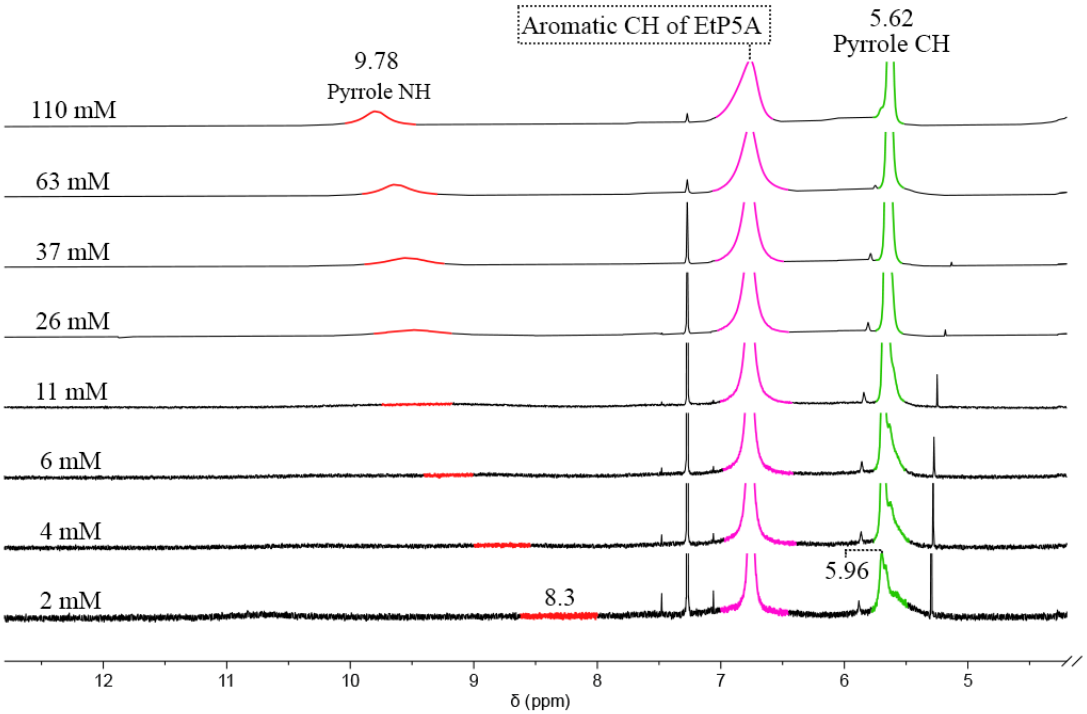

Figure 3.19 : ^{1}H NMR spectra of 1-Br+EtP5A at different concentrations in $CDCl_3$ at 25 °C.

The difference in the molecular translational diffusion can be characterized via diffusion-ordered ^{1}H NMR spectroscopy (DOSY) which will give us an insight into the degree of polymerization. Indisputably, if polymers are present, the value of the diffusion coefficient must be lower than in a system without polymeric structures. For that reason, DOSY of two different concentrations (60 mM and 4 mM) of **1-Br** + **EtP5A** was recorded (Figure 3.20 and 3.21). By increasing the concentration, the value of diffusion coefficient decreased from 4.76×10^{-10} to 2.66×10^{-10} m^2 s^{-1} which indicates the formation of larger aggregates in solution.

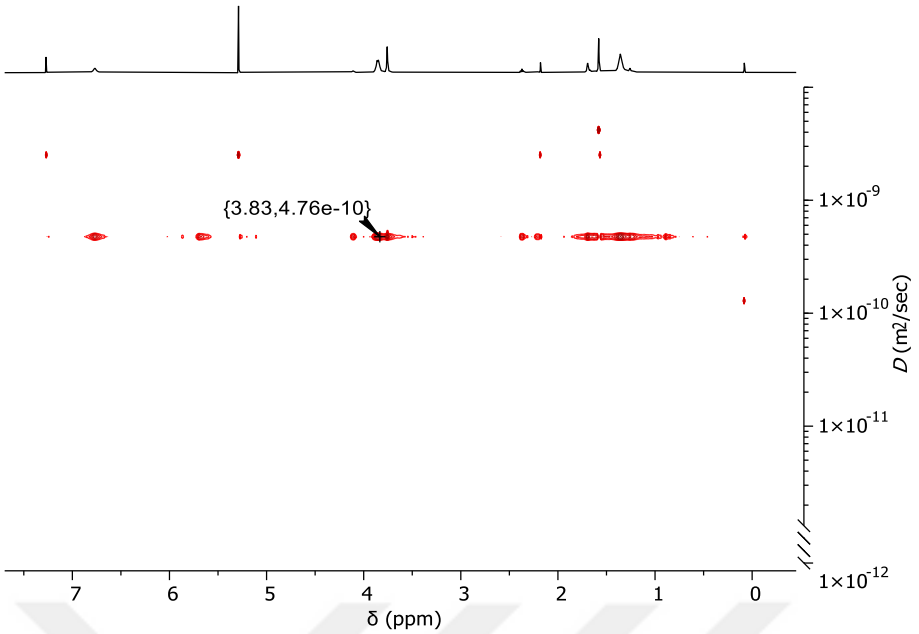

Figure 3.20 : DOSY NMR spectrum of 1-Br and EtP5A (4 mM, $CDCl_3$, 500 MHz, 25 °C).

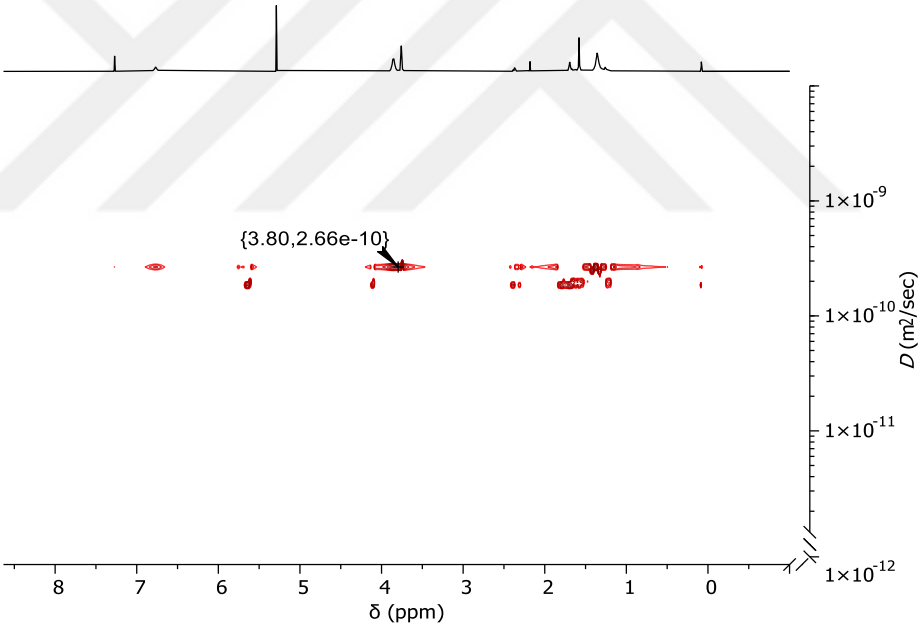

Figure 3.21 : DOSY NMR spectrum of 1-Br and EtP5A (60 mM, $CDCl_3$, 500 MHz, 25 °C).

The double logarithmic curve of specific viscosity (V_s) versus the concentration of monomer (mM) can disclose the system's tendency to polymerization. While the low slope in the specific viscosity (V_s) graph indicates the presence of monomers and oligomers of constant size, the sharp increase in the slope of the linear line above critical polymerization concentration (CPC) is an indication of polymerization. Hence, viscosity measurement supported the poly-pseudorotaxane formation because of the

increase in the slope after CPC (17.6 mM) from 0.82 to 1.37. For this purpose, a 120 mM concentration of **1-Br** and **EtP5A** in chloroform was prepared and by dilution, the values of specific viscosity were determined at room temperature (Figure 3.22).

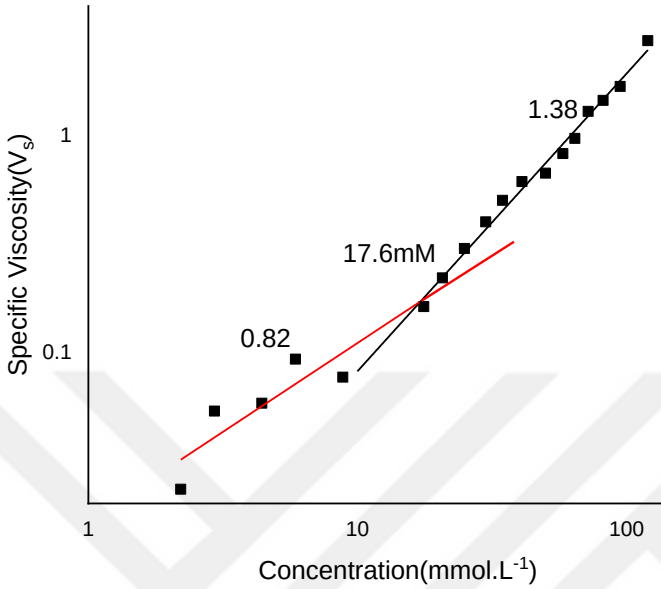

Figure 3.22 : Viscosity-concentration plot of 1-Br + EtP5A in $CHCl_3$ at 25 °C.

A prepared solution of **1-Br** and **EtP5A** (1:1), could depict crystal clear evidence of poly-pseudorotaxane formation using electrospray ionization-mass spectrometry (ESI-MS) (Figure 3.23). Accordingly, the signal at m/z = 1489, corresponds to **[1_2 + Br^-]$^+$**. Furthermore, we were able to see **[1 + EtP5A]** $^+$ and **[1]** $^+$ signals at m/z = 1595 and m/z = 704, respectively which additionally supported the proposed poly-pseudorotaxane structure.

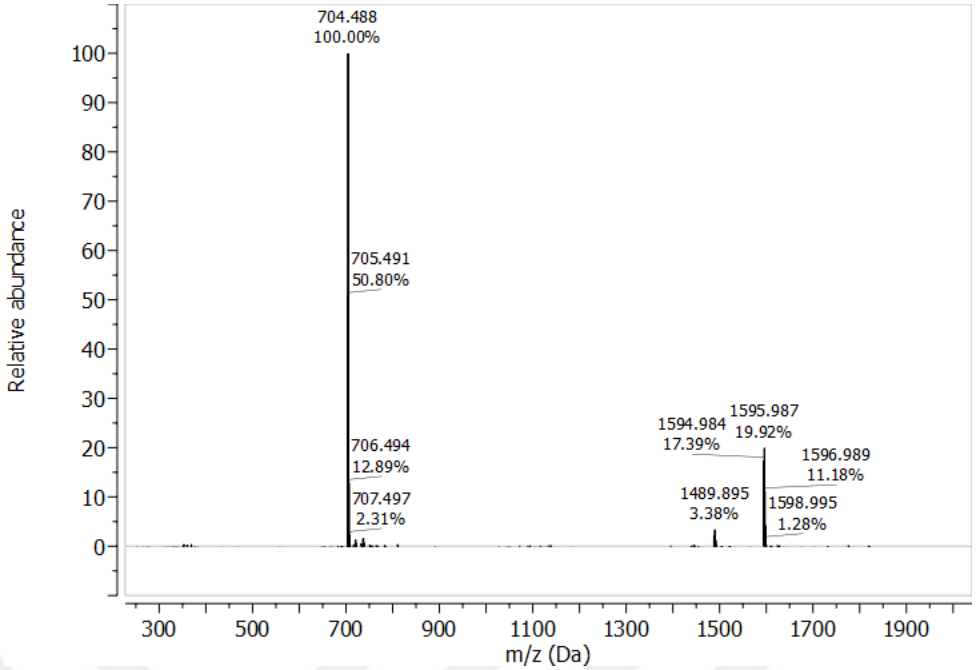

Figure 3.23 : HR-ESIMS of 1-Br + EtP5A.

Furthermore, C4Ps exhibit varying degrees of affinity and stability depending on the type of anions present in the system, which was also examined in our study. We investigated different salts of pyridinium-functionalized calix[4]pyrrole, including pyridinium fluoride (**1-F**), chloride (**1-Cl**), and hexafluorophosphate (**1-PF6**), in addition to its bromide salt (**1-Br**). **C4P** demonstrates the highest affinity towards F^- and Cl^- compared to Br^- and PF_6^- in a poly-pseudorotaxane structure and successful threading of **EtP5A** onto the axle requires weak interactions within the system [32]. Conversely, if Br^- is replaced by F^-, **C4P** retains its cone conformation, stabilizing the structure and promoting stronger cation-π interactions that make the threading of the wheel **EtP5A** more difficult. We validated this hypothesis through ^{1}H NMR by adding an equivalent amount of TBACl and TBAF (1:1) to the mixture of **1-Br** and **EtP5A** at 20 mM (Figure 3.24).

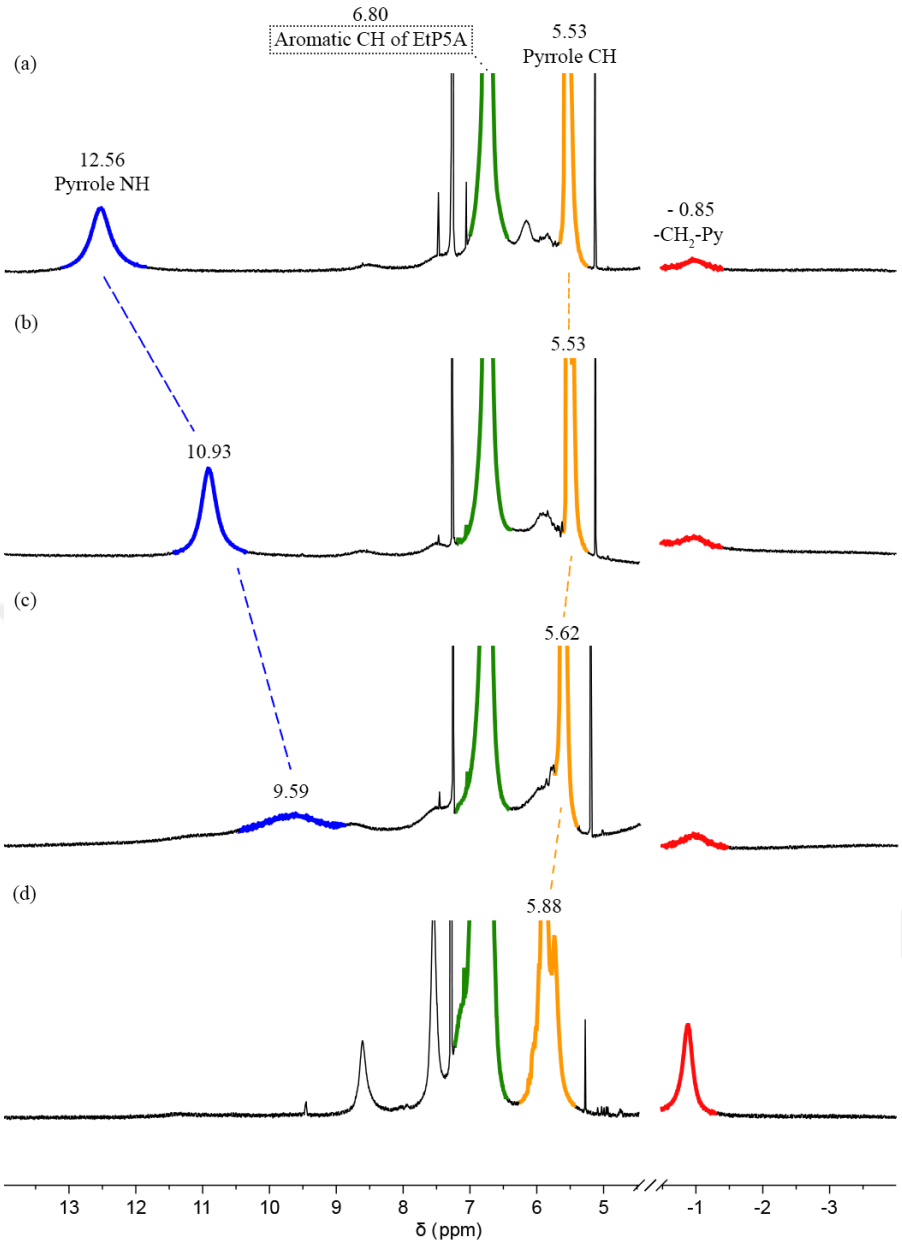

Figure 3.24 : Stacked ^{1}H NMR of (a) 1-F + EtP5A (b) 1-Cl + EtP5A (c) 1-Br + EtP5A and (d) 1-PF6 + EtP5A in $CDCl_3$ at 25 °C.

Consequently, the pyrrolic N-H chemical shift appears at a higher ppm for **1-F**, **1-Cl**, and **1-Br**, respectively, indicating the order of complexation strength between pyrrolic N-H and the corresponding anion, with Br^- and PF_6^- showing the weakest interactions. Also, pyrrolic C-H showed a slightly higher upfield shift in the presence of F^- and Cl^-. Moreover, the aromatic C-H peaks of **EtP5A** display a more broadened peak in the case of **1-Br**, suggesting a more successful threading. Conversely, with PF_6^-, no supramolecular polymerization occurred due to **C4P**'s low affinity towards it, enabling easy threading of **EtP5A**, with significant peak broadening observed. Moreover, the higher ratio of complex peak (**-CH$_2$-Py** at -0.85 ppm) indicated by a higher integration

value in the case of PF_6^- suggested a preference towards pseudorotaxane formation over supramolecular polymerization. On the other hand, the lowest ratio of the corresponding peak in the **1-F** spectrum can be attributed to its low capability in allowing **EtP5A** to be threaded due to the presence of stronger non-covalent interactions in the axle. Therefore, our findings underscore the importance of the type of anion present in controlling poly-pseudorotaxane formation. By understanding the interaction between **C4P** and different anions, we can tailor the formation of supramolecular structures. This evidence was further corroborated by measurements of diffusion coefficients and DLS analysis.

DOSY was performed for a 20 mM mixture possessing different anions (**1-F**, **1-Cl**, **1-Br**, and **1-PF$_6$**) with **EtP5A** which showed a decrease in diffusion coefficients (3.83×10^{-10}, 3.83×10^{-10}, 3.56×10^{-10} and 3.31×10^{-10} m^2 s^{-1}), respectively (Figures 3.25 to 3.28).

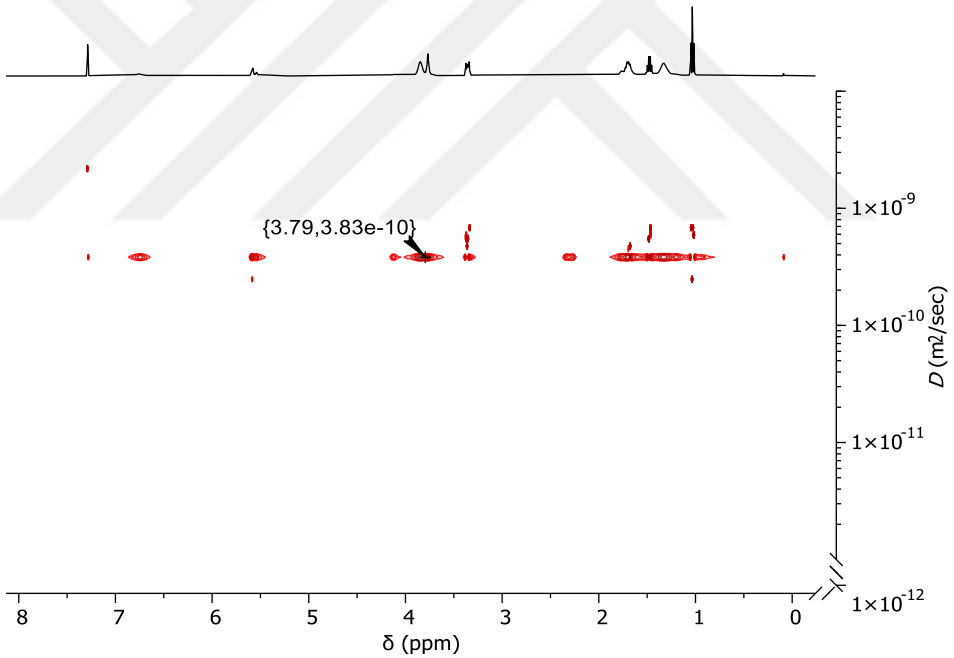

Figure 3.25 : DOSY spectrum of 1-F and EtP5A (20 mM, $CDCl_3$, 500 MHz, 25 °C).

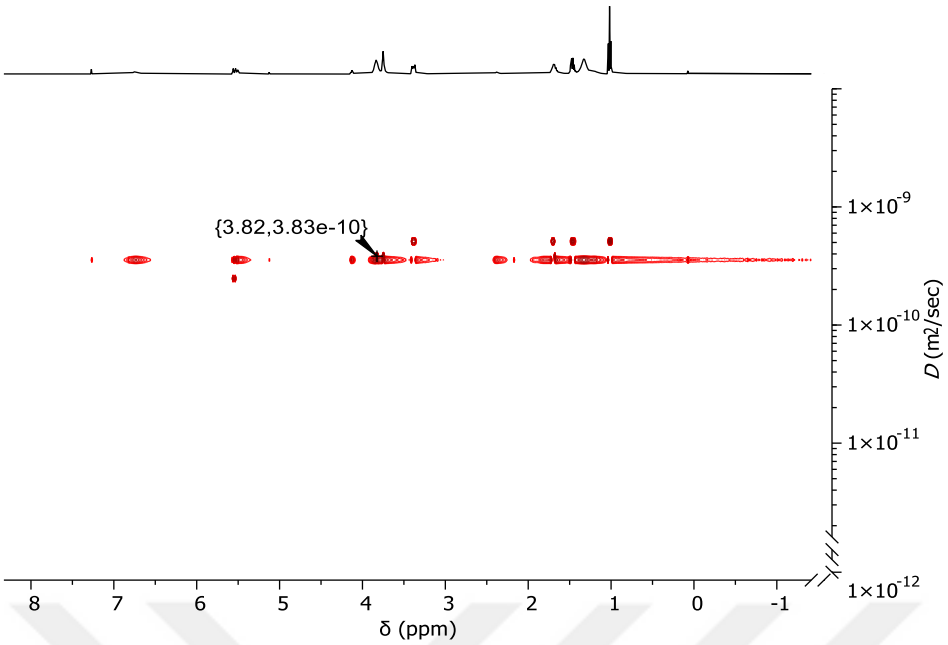

Figure 3.26 : DOSY spectrum of 1-Cl and EtP5A (20 mM, $CDCl_3$, 500 MHz, 25 °C).

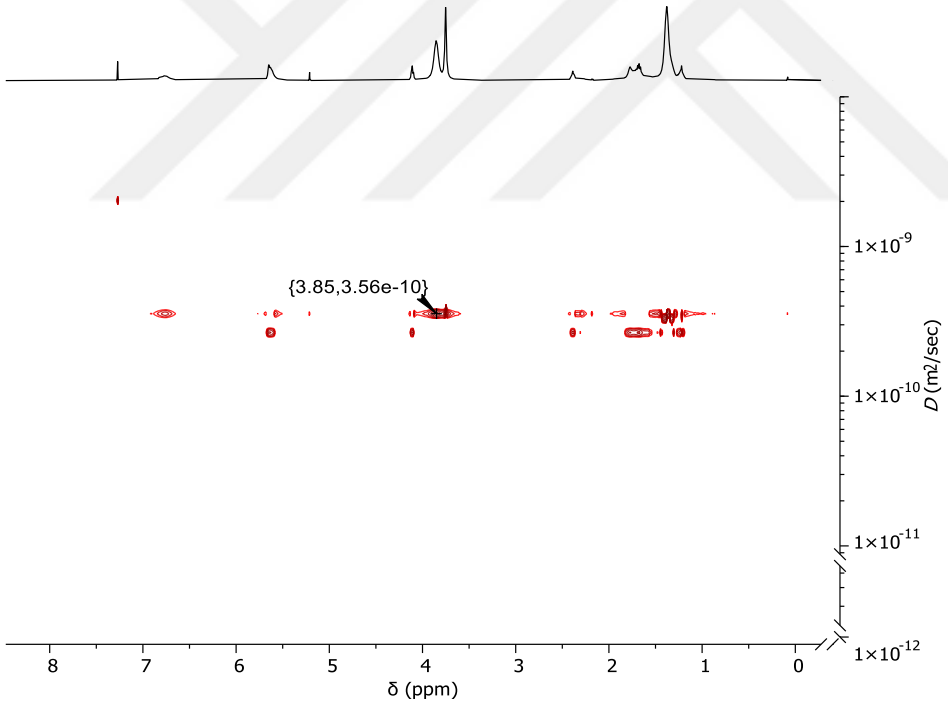

Figure 3.27 : DOSY spectrum of 1-Br and EtP5A (20 mM, $CDCl_3$, 500 MHz, 25 °C).

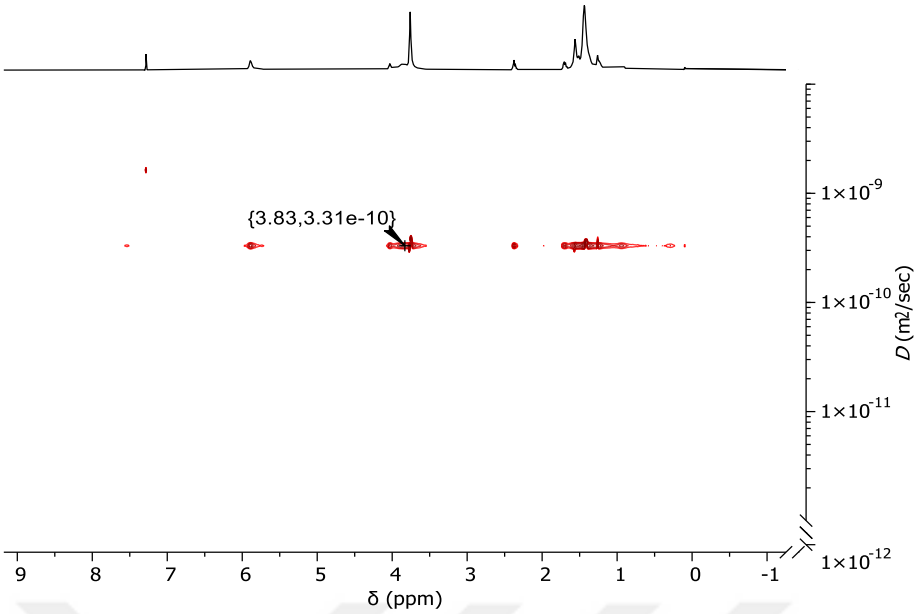

Figure 3.28 : DOSY spectrum of 1-PF6 and EtP5A (20 mM, $CDCl_3$, 500 MHz, 25 °C).

The disparity in diffusion coefficients can be attributed to the selective behavior of **C4P**s towards anions. When weaker interactions occur, such as with Br^- being present, the formation of pseudorotaxanes and subsequent supramolecular polymerization to form poly-pseudorotaxanes becomes more favorable. Conversely, in the case of PF_6^-, the slightly lower diffusion coefficient can be attributed to pseudorotaxane formation without supramolecular polymerization, as there is a lack of anion bonding between **C4P** and PF_6^- because of unfavorable hydrogen bond accepting property of it [34].

The conclusion derived from the DOSY experiments was further reinforced through DLS measurements (Figure 3.29).

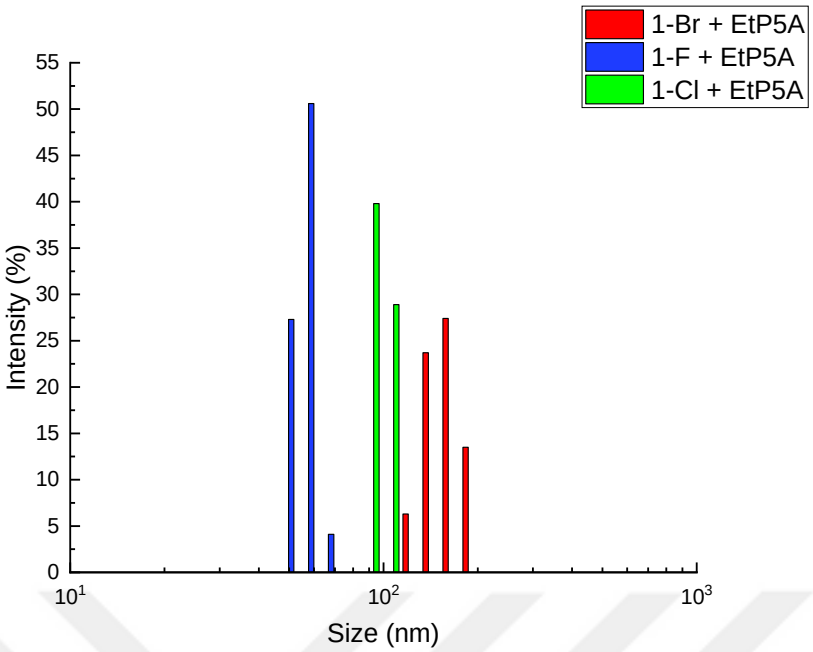

Figure 3.29 : Size distribution bars of poly-pseudorotaxanes using different anions in the system at 40 mM of concentration.

When substituting Br^- with F^- and Cl^-, the selective behavior of **C4P**s led to a decrease in poly-pseudorotaxane formation. Specifically, pseudorotaxane formation was more pronounced in the presence of Br^- due to weaker interactions, facilitating easier threading of **EtP5A** into the axle. Consequently, we anticipate a more favorable pseudorotaxane formation characterized by larger aggregates with a $D_h \approx 160$ nm in the case of the presence of Br^- in the system. The D_h value for Cl^- and F^- salts were found to be 98 and 57 nm, respectively. These results are in good agreement with the previous NMR analyses.

The computational analysis of interaction energies between the pyridinium cation unit and the **C4P** cavity, utilizing various anions in the system, revealed distinct trends both before and after the formation of the poly-pseudorotaxane, facilitated by the introduction of the **EtP5A** parameter (Table 3.1).

Table 3.1 : The interaction energies of pyridinium cation with C4P cavity in the absence/presence of poly-pseudorotaxane molecule and the related structural parameters.

Anions involved in the complexation	Before the addition of EtP5A		After the addition of EtP5A		Δr (Å)	$\Delta(\Delta E_{int})$ (kcal/mol)
	N (Py)… N (C4P) (Å)	ΔE_{int} (kcal/mol)	N (Py)… N (C4P) (Å)	ΔE_{int} (kcal/mol)		
F^-	5.09	-2.05	3.55	-12.3	-1.54	-10.3
Cl^-	5.11	-0.72	3.68	-11.0	-1.43	-10.3
Br^-	5.10	-0.20	3.65	-10.7	-1.45	-10.5
PF_6^-	4.45	-0.95	3.76	-8.40	-0.69	-7.5

Notably, **C4P** exhibits the highest affinity and binding energy with F^-, as evidenced by the most negative interaction energy values, which correspond to stronger interactions. This observation was further supported by the minimal distance between the nitrogen atoms of the pyridinium and **C4P** units. Upon the inclusion of **EtP5A** in the poly-pseudorotaxane formation process, consistent trends persisted. Interestingly, the computation of the change in the change of interaction energy (Δ(ΔEint)) highlighted a significant result: the addition of **EtP5A** induced a reduction in the distance between the nitrogen atoms of pyridinium unit and the **C4P** cavity supporting the stronger cation-π interaction. Consequently, this led to a reinforcement of the interaction between these entities, notably pronounced with bromide displaying a more negative value in Δ(ΔEint) and promoting a more stable structure configuration, accompanied by the release of energy. This finding underscores the remarkable influence of **EtP5A** on the structural and energetic characteristics of the proposed system.

4. CONCLUSIONS

In conclusion, we have successfully synthesized a novel non-ionic surfactant derived from calix[4]pyrrole that is capable of encapsulating DOX·HCl by specifically recognizing its chloride counter anion. This surfactant has shown favorable release properties, particularly in acidic conditions. Moreover, the characteristics and unique drug loading and release capabilities of PEGylated calix[4]pyrrole have been investigated by means of ^{1}H NMR, DLS, TEM, and FT-IR. Additionally, a poly-pseudorotaxane was synthesized utilizing the ion-pair recognition capability of calix[4]pyrrole as the axle and successfully threaded perethylated pillar[5]arene onto the established axle via non-covalent interactions. To validate our proposed structure, we employed various characterization methods such as NMR, viscosity measurement, DLS, and mass spectrometry. Further validation was achieved through an anion-controlled study, which provided insights into structural changes. This thesis presents the first example of a non-ionic surfactant based on calix[4]pyrrole's anion recognition that was successfully incorporated in drug loading and release assays. Moreover, the proposed poly-pseudorotaxane structure has shown good solubility in organic solvents which overcomes one of the most important challenges in rotaxane and pseudorotaxane studies.

REFERENCES

[1] **Bellavita, R., Braccia, S., Falanga, A., & Galdiero, S.** (2023). An Overview of Supramolecular Platforms Boosting Drug Delivery. *Bioinorganic Chemistry and Applications*, *2023*.

[2] **Talreja, S., & Tiwari, S.** (2023). Supramolecular Chemistry: Unveiling the Fascinating World of Non-Covalent Interactions and Complex Assemblies. *Journal of Pharmacy and Pharmacology Research*, ***7***(3), 133–139.

[3] **Davis, A. V., Yeh, R. M., & Raymond, K. N**. (2002). Supramolecular assembly dynamics. *Proceedings of the National Academy of Sciences*, ***99***(8), 4793-4796.

[4] **Gao, L., Zheng, B., Chen, W., & Schalley, C. A**. (2015). Enzyme-responsive pillar[5]arene-based polymer-substituted amphiphiles: synthesis, self-assembly in water, and application in controlled drug release. *Chemical Communications*, ***51***(80), 14901–14904.

[5] **Mao, W., & Ma, D.** (2020). Stimuli-Responsive Self-Assembly Based on Macrocyclic Hosts and Biomedical Applications. *Handbook of Macrocyclic Supramolecular Assembly*, 603-646.

[6] **Menger, F. M.** (2002). Supramolecular chemistry and self-assembly. *Proceedings of the National Academy of Sciences of the United States of America*, ***99***(8), 4818–4822.

[7] **Corrie, P. G**. (2008). Cytotoxic chemotherapy: clinical aspects. *Medicine*, ***36***(1), 24-28.

[8] **Torchilin, V. P.** (2001). Structure and design of polymeric surfactant-based drug delivery systems. *Journal of Controlled Release*, ***73***(2-3), 137–172.

[9] **Pawar, A., Kamdi, V., Alaspure, A., & Gangane, P.** (2022). Recent Updates on Polymeric Micelles: A Review. *International Journal of Pharmaceutical Sciences Review and Research*, 37–52.

[10] **An, L., Wang, Y., Liu, X., Ma, N., Du, H., Jin, M., Liu, Y., Zhang, L., Xu, Y., Huang, P., & Sun, Z.** (2011). Block Ionomer Complex Micelles Based on the Self-Assembly of Poly(ethylene glycol)-block-poly(acrylic acid) and CdCl2 for Anti-tumor Drug Delivery. *Chemical & Pharmaceutical Bulletin/Chemical and Pharmaceutical Bulletin*, ***59***(5), 559–563.

[11] **Xue, M., Yang, Y., Chi, X., Yan, X., & Huang, F.** (2015). Development of Pseudorotaxanes and Rotaxanes: From Synthesis to Stimuli-Responsive Motions to Applications. *Chemical Reviews*, ***115***(15), 7398–7501.

[12] **Aydogan, A., & Sessler, J. L.** (2014). An imidazolium-functionalized self-assembling calix[4]pyrrole. *Chemical communications*, ***50***(88), 13600-13603.

[13] **Valderrey, V., Escudero-Adán, E. C., & Ballester, P**. (2012). Polyatomic Anion Assistance in the Assembly of [2]Pseudorotaxanes. *Journal of the American Chemical Society*, ***134***(26), 10733–10736.

[14] **Bektas, N., & Aydogan, A.** (2023). A poly-pseudorotaxane constructed by threading pillar[5]arene onto an ion-pair recognition-based calix[4]pyrrole supramolecular polymer. *Organic & Biomolecular Chemistry*, ***21***(9), 1862–1867.

[15] **Kim, D. S., & Sessler, J. L.** (2015). Calix [4] pyrroles: versatile molecular containers with ion transport, recognition, and molecular switching functions. *Chemical Society Reviews*, ***44***(2), 532-546.

[16] **Rather, I. A., Wagay, S. A., Hasnain, M. S., & Ali, R.** (2019). New dimensions in calix[4]pyrrole: the land of opportunity in supramolecular chemistry. *RSC Advances*, ***9***(66), 38309–38344.

[17] **Sung Wan Kim, & Sessler, J. L.** (2014). Calix[4]pyrrole-Based Ion Pair Receptors. *Accounts of Chemical Research*, ***47***(8), 2525–2536.

[18] **Sessler, J. L., Gale, P. A., & Genge, J. W.** (1998). Calix [4] pyrroles: New solid-phase HPLC supports for the separation of anions. *Chemistry–A European Journal*, ***4***(6), 1095-1099.

[19] **Grazia Cafeo, Grazia Carbotti, Cuzzola, A., Fabbi, M., Ferrini, S., Kohnke, F. H., Papanikolaou, G., Maria Rosaria Plutino, Rosano, C., & Andrew.** (2013). Drug Delivery with a Calixpyrrole–*trans*-Pt(II) Complex. *Journal of the American Chemical Society*, ***135***(7), 2544–2551.

[20] **Geretto, M., Ponassi, M., Casale, M., Pulliero, A., Cafeo, G., Malagreca, F., Profumo, A., Balza, E., Bersimbaev, R., Kohnke, F. H., Rosano, C., & Izzotti, A.** (2018). A novel calix[4]pyrrole derivative as a potential anticancer agent that forms genotoxic adducts with DNA. *Scientific Reports*, ***8***(1), 11075.

[21] **Gao, L., Zheng, B., Chen, W., & Schalley, C. A.** (2015). Enzyme-responsive pillar[5]arene-based polymer-substituted amphiphiles: synthesis, self-assembly in water, and application in controlled drug release. *Chemical Communications*, ***51***(80), 14901–14904.

[22] **Cui, Y. H., Deng, R., Li, Z., Du, X. S., Jia, Q., Wang, X. H., ... & Yang, Y. W.** (2019). Pillar [5] arene pseudo [1] rotaxane-based redox-responsive supramolecular vesicles for controlled drug release. *Materials Chemistry Frontiers*, ***3***(7), 1427-1432.

[23] **Ji, X., Guo, C., Chen, W., Long, L., Zhang, G., Khashab, N. M., & Sessler, J. L.** (2018). Removal of anions from aqueous media by means of a thermoresponsive calix [4] pyrrole amphiphilic polymer. *Chemistry–A European Journal*, ***24***(59), 15791-15795.

[24] **Chen, H., Chen, Y., Wu, H., Xu, J. F., Sun, Z., & Zhang, X.** (2018). Supramolecular polymeric chemotherapy based on cucurbit [7] uril-PEG copolymer. *Biomaterials*, ***178***, 697-705.

[25] **Chi, X., Peters, G. M., Hammel, F., Brockman, C., & Sessler, J. L.** (2017). Molecular recognition under interfacial conditions: Calix [4] pyrrole-based cross-linkable micelles for ion pair extraction. *Journal of the American Chemical Society*, ***139***(27), 9124-9127.

[26] **Xia, D., Lv, X., Chen, K., & Wang, P.** (2019). A [2]pseudorotaxane based on a pillar[6]arene and its application in the construction of a metallosupramolecular polymer. *Dalton Transactions*, ***48***(27), 9954–9958.

[27] **Arunachalam, M., & Gibson, H. W.** (2014). *Recent developments in polypseudorotaxanes and polyrotaxanes*. ***39***(6), 1043–1073.

[28] **Sun, S., Hu, X.-Y., Chen, D., Shi, J., Dong, Y., Lin, C., Pan, Y., & Wang, L.** (2013). Pillar[5]arene-based side-chain polypseudorotaxanes as an anion-responsive fluorescent sensor. *Polymer Chemistry*, ***4***(7), 2224.

[29] **Su, H., Chen, W., Li, L., Li, B., Zhang, Z.-Y., & Li, C.** (2020). Coordination-Driven Poly[2]Pseudorotaxanes in Highly Polar Organic Solvent. *Frontiers in Chemistry*, ***8***, 579.

[30] **Budak, A., & Aydogan, A**. (2021). A calix[4]pyrrole-based linear supramolecular polymer constructed by orthogonal self-assembly. *Chemical Communications*, ***57***(34), 4186–4189.

[31] **Ogoshi, T., Kitajima, K., Aoki, T., Fujinami, S., Yamagishi, T. A., & Nakamoto, Y.** (2010). Synthesis and conformational characteristics of alkyl-substituted pillar [5] arenes. *The Journal of Organic Chemistry*, ***75***(10), 3268-3273.

[32] **Joy, F., Nizam, A., Nair, Y., Pillai, Renjith. S., Devasia, J., & Praveen Nagella.** (2022). Templating motifs of molecular axles in hydrogen bonding [2]rotaxanes: Synthesis and applications. ***181***, 111696–111696.

[33] **Moisanu, C. M., Jacobberger, R. M., Skala, L. P., Stern, C. L., Wasielewski, M. R., & Dichtel, W. R.** (2023). Crystalline Arrays of Copper Porphyrin Qubits Based on Ion-Paired Frameworks. *Journal of the American Chemical Society*, ***145***(33), 18447-18454.

[34] **Gross, D. E., Schmidtchen, F. P., Antonius, W., Gale, P. A., Lynch, V. M., & Sessler, J. L**. (2008). Cooperative binding of calix [4] pyrrole–anion complexes and alkylammonium cations in halogenated solvents. *Chemistry–A European Journal*, ***14***(26), 7822-7827.

CURRICULUM VITAE

Name Surname **: Mana MIRABOLGHASEMI**

EDUCATION **:**

- **B.Sc.** **:** 2017, Alzahra University, Faculty of Physics and Chemistry, Chemistry Department

PUBLICATION AND PRESENTATION ON THE THESIS:

- **Mirabolghasemi, M., Bektas, N., Sancakli, B., Dag, A. and Aydogan, A.**, 2024: Drug Encapsulation and Release with A Non-Ionic Amphiphilic calix[4]pyrrole. 3rd International Graduate Research Symposium (IGRS'24), May 8-10, Istanbul, Turkey.
- **Mirabolghasemi, M., Bektas, N., Sancakli, B., Dag, A., & Aydogan, A.** (2024). Drug encapsulation and release with a nonionic amphiphilic calix [4] pyrrole. *New Journal of Chemistry*.